

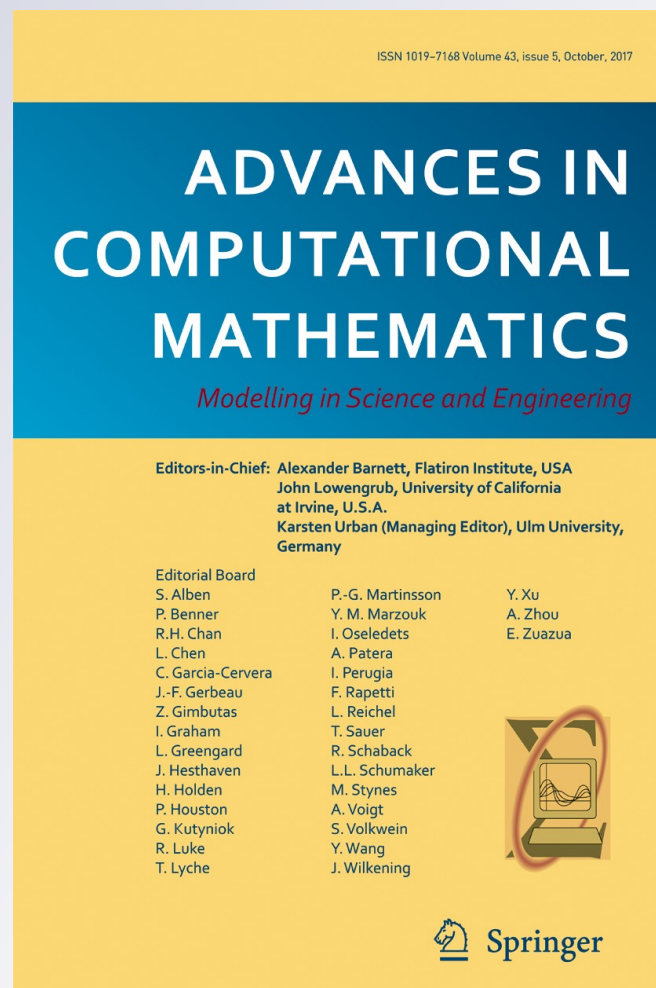
Dimension-by-dimension moment-based central Hermite WENO schemes for directly solving Hamilton-Jacobi equations

Zhanjing Tao & Jianxian Qiu

Advances in Computational Mathematics
Modelling in Science and Engineering

ISSN 1019-7168
Volume 43
Number 5


Adv Comput Math (2017) 43:1023-1058
DOI 10.1007/s10444-017-9515-2



Your article is protected by copyright and all rights are held exclusively by Springer Science +Business Media New York. This e-offprint is for personal use only and shall not be self-archived in electronic repositories. If you wish to self-archive your article, please use the accepted manuscript version for posting on your own website. You may further deposit the accepted manuscript version in any repository, provided it is only made publicly available 12 months after official publication or later and provided acknowledgement is given to the original source of publication and a link is inserted to the published article on Springer's website. The link must be accompanied by the following text: "The final publication is available at link.springer.com".



Dimension-by-dimension moment-based central Hermite WENO schemes for directly solving Hamilton-Jacobi equations

Zhanjing Tao^{1,2} · Jianxian Qiu¹ 

Received: 16 January 2016 / Accepted: 17 January 2017/

Published online: 4 February 2017

© Springer Science+Business Media New York 2017

Abstract In this paper, a class of high-order central Hermite WENO (HWENO) schemes based on finite volume framework and staggered meshes is proposed for directly solving one- and two-dimensional Hamilton-Jacobi (HJ) equations. The methods involve the Lax-Wendroff type discretizations or the natural continuous extension of Runge-Kutta methods in time. This work can be regarded as an extension of central HWENO schemes for hyperbolic conservation laws (Tao et al. *J. Comput. Phys.* **318**, 222–251, 2016) which combine the central scheme and the HWENO spatial reconstructions and therefore carry many features of both schemes. Generally, it is not straightforward to design a finite volume scheme to directly solve HJ equations and a key ingredient for directly solving such equations is the reconstruction of numerical Hamiltonians to guarantee the stability of methods. Benefited from the central strategy, our methods require no numerical Hamiltonians. Meanwhile, the zeroth-order and the first-order moments of the solution are involved in the spatial HWENO reconstructions which is more compact compared with WENO schemes. The reconstructions are implemented through a dimension-by-dimension strategy when the spatial dimension is higher than one. A collection of one- and two-dimensional numerical examples is performed to validate high resolution and robustness

Communicated by: Helge Holden

✉ Jianxian Qiu
jxqiu@xmu.edu.cn

Zhanjing Tao
tzjnchy555@163.com

¹ School of Mathematical Sciences and Fujian Provincial Key Laboratory of Mathematical Modeling and High-Performance Scientific Computing, Xiamen University, Xiamen, Fujian, 361005, People's Republic of China

² Present address: Department of Mathematics, Michigan State University, East Lansing, MI 48824, USA

of the methods in approximating the solutions of HJ equations, which involve linear, nonlinear, smooth, non-smooth, convex or non-convex Hamiltonians.

Keywords Finite volume method · Central scheme · Hamilton-Jacobi equation; Hermite WENO · Lax-Wendroff · Natural continuous extension (NCE) of Runge-Kutta

Mathematics Subject Classification (2010) 65M60 · 35L65

1 Introduction

In this paper, we propose a class of finite volume central Hermite WENO (weighted essentially non-oscillatory, C-HWENO) schemes for directly simulating one- and two-dimensional Hamilton-Jacobi (HJ) equations:

$$\begin{cases} \phi_t + H(\nabla_x \phi) = 0, \\ \phi(x, 0) = \phi_0(x), \end{cases} \quad (1.1)$$

with suitable initial and boundary conditions and H is the Hamiltonian. Here (1.1) can involve linear, nonlinear, smooth, non-smooth, convex or non-convex Hamiltonians. The HJ equations arise in various applications in science and engineering, such as optimal control, geometric optics, image processing, seismic waves, crystal growth and robotic navigation. In general the solutions of such equations are continuous but may develop discontinuous derivatives in finite time regardless of the smoothness of the initial and boundary data. To ensure the existence of the solution as well as to single out the physical relevant solution, the concept of viscosity solution was established mainly by Crandall, Evans and Lions [9, 10] for HJ equations.

There are various accurate and robust numerical methods for solving HJ equations. Many methods are based on the close relation between HJ equations and conservation laws. Note that by differentiating (1.1) with respect to x , one can obtain a conservation system for $\nabla_x \phi$,

$$(\nabla_x \phi)_t + \nabla_x H(\nabla_x \phi) = 0$$

Hence successful numerical methods for conservation laws can be adapted for solving the HJ equations. Osher and Sethian [26] presented a second-order essentially non-oscillatory (ENO) scheme, and Osher and Shu [27] constructed high-order ENO schemes to solve the HJ equations. In [14], the original WENO with Runge-Kutta time discretization schemes for HJ equations was proposed by Jiang and Peng. Later, Qiu and Shu [29, 30] proposed the HWENO schemes based on Runge-Kutta and the Lax-Wendroff time discretizations for HJ equations. Based on unstructured meshes, Lafon and Osher [17] constructed ENO schemes for solving HJ equations. Zhang and Shu [36], Li and Chan [21] further developed high-order WENO schemes for solving two-dimensional HJ equations on triangular meshes. Besides, some finite element methods for arbitrary triangular meshes were designed in [1, 2, 13, 19]. For a detailed review of high-order numerical methods for HJ equations, we refer to the lecture note [31].

An alternative approach is solving HJ equations directly. Cheng and Shu presented DG methods to directly solve HJ equations for ϕ and a new Hamiltonian was designed to keep stability of the method in [7]. Later, a new local DG method to directly solve HJ equations was developed by Yan and Osher [34]. In [8], Cheng and Wang also improved their early work by utilizing the Roe speed at the cell interface and proposed an entropy fix by adding penalty terms based on structured and unstructured meshes. Recently, Zheng and Qiu [37] developed Hermite WENO schemes to directly solve the HJ equations.

Based on the simplicity and robustness of central schemes, there are also many high resolution central schemes for HJ equations analogous to ones for conservation laws. Lin and Tadmor applied these central ideas to HJ equations in [22]. There, first- and second-order staggered schemes were written in one and two dimensions. An L^1 convergence of order one for this scheme was proven in [23]. Later, a second-order semi-discrete scheme for HJ equations was introduced by Kurganov and Tadmor [16]. Bryson and Levy developed in [4] new and efficient central schemes which were first- and second-order accurate and were designed to scale well with an increasing dimension for multidimensional HJ equations. After that, the third- and fifth-order central schemes and the fifth-order semi-discrete central-upwind methods based on WENO reconstructions for approximating the solutions of multidimensional HJ equations were presented in [5] and [6], respectively. Recently, Li and Yakovlev [20] proposed a central discontinuous Galerkin method to solve for the viscosity solutions of HJ equations. It is well known that the reconstruction of numerical Hamiltonians is the key ingredient to directly solve HJ equations in upwind methods and the main advantage of the central scheme is requiring no (approximate) Riemann solvers or numerical Hamiltonians. Motivated by this, the methods in this paper are formulated in a central framework which leads to a simple formulation for the Hamiltonian.

The work in this paper is an extension of the C-HWENO methods for hyperbolic conservation laws in [33] to HJ equations. Like all WENO-type methods, the C-HWENO methods are accurate and essentially non-oscillatory. We use the same Hermite WENO (HWENO) spatial reconstructions as in [33] which are based on the zeroth-order and first-order moments of the solution rather than the solution and its derivative(s) in [32]. Compared with WENO schemes, one major advantage of HWENO schemes is the compactness in the reconstruction. Using moments of the solution itself is not new in HWENO reconstruction [11, 25], one novel aspect of our strategy is to involve all the first-order moments, including the mixed-type moment (see $\overline{v w}_{ij}^n$ in Section 2.2), of the solution, when the spatial dimension is higher than one. Working with such choice of the moments enables a dimension-by-dimension procedure for the reconstructions, a core ingredient of the proposed methods. Since our proposed schemes are of fully discrete, the time derivative term must also be discretized. Motivated by WENO or HWENO schemes for HJ equations [28, 29], we apply the Lax-Wendroff type discretizations [12, 18] for the time discretizations. Alternatively, we also apply the natural continuous extension of Runge-Kutta methods [35] in time following the line of lots of central schemes.

The organization of this paper is as follows. In Section 2, we review and present the construction and implementation of the proposed C-HWENO schemes based on moments of the solution with Lax-Wendroff type time discretizations for the problem

(1.1) in one and two dimensions. The two-dimensional spatial reconstructions are implemented in a dimension-by-dimension fashion. In Section 3, we review and design the construction and implementation of the proposed C-HWENO schemes with the natural continuous extension of Runge-Kutta methods as time discretizations, and the WENO reconstructions are used for the computation of flux of the Runge-Kutta methods. In Section 4, we report on extensive numerical examples to demonstrate the performance of the proposed schemes. Concluding remarks are given in Section 5.

2 Central Hermite WENO schemes with Lax-Wendroff time discretization

In this section we describe the framework of central Hermite WENO (HWENO) schemes with fifth-order spatial reconstructions and Lax-Wendroff time discretizations for one- and two-dimensional Hamilton-Jacobi equations.

2.1 One-dimensional case

Consider the one-dimensional Hamilton-Jacobi equation

$$\begin{cases} \phi_t + H(\phi_x) = 0, \\ \phi(x, 0) = \phi_0(x). \end{cases} \tag{2.1}$$

The proposed numerical method will be defined on staggered meshes. For simplicity of presentation, uniform meshes are used with the mesh size Δx . Each cell of the *primal* mesh is denoted as $I_i = [x_{i-1/2}, x_{i+1/2}]$ with its cell center $x_i = \frac{1}{2}(x_{i-1/2} + x_{i+1/2})$; and each cell of the *dual* mesh is denoted as $I_{i+1/2} = [x_i, x_{i+1}]$ with its cell center $x_{i+1/2} = \frac{1}{2}(x_i + x_{i+1})$. It will be seen that the primal and the dual meshes will be used in a staggered fashion along the time direction in the proposed scheme.

Multiplying a locally scaled polynomial $\frac{x-x_c}{\Delta x}$ of degree one to Eq. 2.1, we also obtain a relation for the first-order moment of the solution,

$$\phi_t \frac{x - x_c}{\Delta x} + H(\phi_x) \frac{x - x_c}{\Delta x} = 0 \tag{2.2}$$

where x_c is the center of the relevant mesh element. In particular, for a cell from the primal mesh, we will take $x_c = x_i$ with some i ; for a cell from the dual mesh, we will take $x_c = x_{i+1/2}$ with some i .

Now we apply the staggered central scheme strategy to Eqs. 2.1 and 2.2. Suppose at $t = t^n$, the approximations for the first two moments of the solution, denoted as $\{\bar{\phi}_i^n\}$ and $\{\bar{v}_i^n\}$, are available on the primal mesh, that is, $\forall i$,

$$\bar{\phi}_i^n \approx \frac{1}{\Delta x} \int_{I_i} \phi(x, t^n) dx, \quad \bar{v}_i^n \approx \frac{1}{\Delta x} \int_{I_i} \phi(x, t^n) \frac{x - x_i}{\Delta x} dx.$$

- (a.1) We integrate Eqs. 2.1 and 2.2 over $[t^n, t^{n+1}] \times [x_i, x_{i+1}]$, and approximate the first two moments of the solution associated with the dual mesh at $t^{n+1} = t^n + \Delta t$ as below,

$$\bar{\phi}_{i+1/2}^{n+1} = \bar{\phi}_{i+1/2}^n - \frac{1}{\Delta x} \int_{t^n}^{t^{n+1}} \int_{x_i}^{x_{i+1}} H(\phi_x(x, t)) dx dt, \tag{2.3}$$

$$\bar{v}_{i+1/2}^{n+1} = \bar{v}_{i+1/2}^n - \frac{1}{\Delta x} \int_{t^n}^{t^{n+1}} \int_{x_i}^{x_{i+1}} H(\phi_x(x, t)) \frac{x - x_{i+1/2}}{\Delta x} dx dt. \tag{2.4}$$

All the terms on the right-hand side of Eqs. 2.3–2.4 will be reconstructed based on $\{\bar{\phi}_i^n, \bar{v}_i^n\}_i$. For simplicity of notation, we still use ϕ in the above relations, though it is no longer the exact solution.

- (a.2) We then integrate Eqs. 2.1 and 2.2 over $[t^{n+1}, t^{n+2}] \times [x_{i-1/2}, x_{i+1/2}]$, and continue to approximate the first two moments of the solution with respect to the primal mesh at $t^{n+2} = t^{n+1} + \Delta t$,

$$\begin{aligned} \bar{\phi}_i^{n+2} &= \bar{\phi}_i^{n+1} - \frac{1}{\Delta x} \int_{t^{n+1}}^{t^{n+2}} \int_{x_{i-1/2}}^{x_{i+1/2}} H(\phi_x(x, t)) dx dt, \\ \bar{v}_i^{n+2} &= \bar{v}_i^{n+1} - \frac{1}{\Delta x} \int_{t^{n+1}}^{t^{n+2}} \int_{x_{i-1/2}}^{x_{i+1/2}} H(\phi_x(x, t)) \frac{x - x_i}{\Delta x} dx dt. \end{aligned}$$

- (a.3) Set n to be $n + 2$, and go to (a.1).

Note that the moments are defined and evolved in a staggered fashion with respect to the discrete time level n on two sets of meshes. The mesh switches back after two time steps.

The remaining of this section will be mainly devoted to the details to update from t^n to t^{n+1} according to Eqs. 2.3 and 2.4. Since we will propose a fifth-order central HWENO (C-HWENO) method, with this in mind, we further approximate the spatial integral in Eqs. 2.3 and 2.4 with the four-point Gauss-Lobatto quadrature formula,

$$\bar{\phi}_{i+1/2}^{n+1} = \bar{\phi}_{i+1/2}^n - \sum_{l=1}^4 \omega_l \int_{t^n}^{t^{n+1}} H(\phi_x(\mathcal{G}_l^x, t)) dt, \tag{2.5}$$

$$\bar{v}_{i+1/2}^{n+1} = \bar{v}_{i+1/2}^n - \sum_{l=1}^4 \omega_l \frac{\mathcal{G}_l^x - x_{i+1/2}}{\Delta x} \int_{t^n}^{t^{n+1}} H(\phi_x(\mathcal{G}_l^x, t)) dt, \tag{2.6}$$

where $\{\omega_l\}_{l=1}^4$ are Gauss-Lobatto quadrature weights

$$\omega_1 = \omega_4 = \frac{1}{12}, \quad \omega_2 = \omega_3 = \frac{5}{12},$$

and

$$\mathcal{G}_1^x = x_i, \quad \mathcal{G}_2^x = x_{i+\frac{1}{2}-\frac{\sqrt{5}}{10}}, \quad \mathcal{G}_3^x = x_{i+\frac{1}{2}+\frac{\sqrt{5}}{10}}, \quad \mathcal{G}_4^x = x_{i+1}, \tag{2.7}$$

are the Gauss-Lobatto quadrature points over the cell $I_{i+1/2} = [x_i, x_{i+1}]$. In the target cell I_i of the primal mesh, such quadrature points are denoted as

$$\mathcal{G}^{x,i} = \{x_{i-\frac{1}{2}+\frac{\sqrt{5}}{10}}, x_i, x_{i+\frac{1}{2}-\frac{\sqrt{5}}{10}}\}.$$

If we consider the problem (2.1) with the piecewise initial data $\phi|_{t_i} = \bar{\phi}_i^n$ at t^n , under the assumption that the time step Δt satisfies a CFL restriction $\Delta t \leq \frac{C_{cfl} \Delta x}{\max_i |H'(\phi_x(x_i, t^n))|}$ with some constant C_{cfl} and $H'(\phi_x(x_i, t^n))$ being the characteristic speed of Eq. 2.1, the discontinuities starting at t^n from $x_{i-\frac{1}{2}}$ and $x_{i+\frac{1}{2}}$ will not propagate to x_* with $x_* \in \mathcal{G}^{x,i}$ over a single time step Δt , and therefore the solution of this problem restricted at x_* with $x_* \in \mathcal{G}^{x,i}$, $\forall i$ are smooth for $t \in [t^n, t^{n+1}]$. Motivated by this, the Hamiltonian function $H(\phi_x(x_*, t))$ in Eqs. 2.5 and 2.6 can be approximated by a temporal Taylor expansion at t^n according to the following

$$H(\phi_x(x_*, t)) \approx H(\phi_x(x_*, t^n)) + (t-t^n) \frac{\partial}{\partial t} H(\phi_x(x_*, t^n)) + \frac{(t-t^n)^2}{2} \frac{\partial^2}{\partial t^2} H(\phi_x(x_*, t^n)). \tag{2.8}$$

If we want to obtain the $(k + 1)$ th-order accuracy in time, we need to approximate the first k time derivatives: $\frac{\partial}{\partial t} H, \dots, \frac{\partial^k}{\partial t^k} H$. In this paper, we will proceed up to the third-order accuracy in time, although the procedure can be extended directly to any other order.

Plugging the relation (2.8) into Eqs. 2.5 and 2.6, this will lead to our actual update formulations

$$\bar{\phi}_{i+1/2}^{n+1} = \bar{\phi}_{i+1/2}^n - \sum_{l=1}^4 \omega_l F(\phi(\mathcal{G}_l^x, t^n)), \tag{2.9}$$

$$\bar{v}_{i+1/2}^{n+1} = \bar{v}_{i+1/2}^n - \sum_{l=1}^4 \omega_l F(\phi(\mathcal{G}_l^x, t^n)) \frac{\mathcal{G}_l^x - x_{i+1/2}}{\Delta x}, \tag{2.10}$$

with

$$F = F(\phi) = \Delta t H + \frac{\Delta t^2}{2} \frac{\partial}{\partial t} H + \frac{\Delta t^3}{6} \frac{\partial^2}{\partial t^2} H = \Delta t H + \frac{\Delta t^2}{2} H' \phi_{xt} + \frac{\Delta t^3}{6} (H'' \phi_{xt}^2 + H' \phi_{xtt}), \tag{2.11}$$

Next we convert the temporal derivative terms of ϕ in Eq. 2.11 into spatial ones by repeatedly using the governing equation (2.1):

$$\begin{aligned} \phi_{xt} &= (\phi_t)_x = -H'(\phi_x) \phi_{xx}, \\ \phi_{xtt} &= (\phi_{tt})_x = 2H''(\phi_x) H'(\phi_x) \phi_{xx}^2 + (H'(\phi_x))^2 \phi_{xxx}. \end{aligned} \tag{2.12}$$

Even though $F(\phi)$ is used throughout the presentation, one should keep in mind that we indeed have $F = \mathcal{F}(\phi_x, \phi_{xx}, \phi_{xxx})$.

Specifically, to obtain the moments $\bar{\phi}_{i+1/2}^{n+1}$ and $\bar{v}_{i+1/2}^{n+1}$ on the dual mesh at the next time t^{n+1} according to Eqs. 2.9 and 2.10, one will need to reconstruct at the current time t^n , $\forall i$,

- (1) the moments $\bar{\phi}_{i+1/2}^n, \bar{v}_{i+1/2}^n$ on the dual mesh, as well as
- (2) the point value of $q(x_*, t^n)$, where $q = \phi_x, \phi_{xx}$, or ϕ_{xxx} , and $x_* \in \mathcal{G}^{x,i}$,

based on the given data $\{\bar{\phi}_i^n, \bar{v}_i^n\}_i$.

On the other hand,

$$\bar{\phi}_{i+1/2}^n \approx \frac{1}{\Delta x} \int_{x_i}^{x_{i+1}} \phi(x, t^n) dx = \frac{1}{\Delta x} \int_{x_i}^{x_{i+1/2}} \phi(x, t^n) dx + \frac{1}{\Delta x} \int_{x_{i+1/2}}^{x_{i+1}} \phi(x, t^n) dx.$$

This implies that to approximate the moment $\bar{\phi}_{i+1/2}^n$, one would want to get the half-cell moments: $\frac{1}{\Delta x} \int_{x_i}^{x_{i+1/2}} \phi(x, t^n) dx$ and $\frac{1}{\Delta x} \int_{x_{i+1/2}}^{x_{i+1}} \phi(x, t^n) dx$. This is likewise for the moment $\bar{v}_{i+1/2}^n$,

$$\bar{v}_{i+1/2}^n \approx \frac{1}{\Delta x} \int_{x_i}^{x_{i+1/2}} \phi(x, t^n) \frac{x-x_{i+1/2}}{\Delta x} dx + \frac{1}{\Delta x} \int_{x_{i+1/2}}^{x_{i+1}} \phi(x, t^n) \frac{x-x_{i+1/2}}{\Delta x} dx.$$

To reconstruct the half-cell moments and point values mentioned above, we propose a procedure by adopting the one-dimensional fifth-order accurate HWENO reconstruction in central Hermite WENO methods for hyperbolic conservation laws we developed previously. For more details we refer to [33], and shall not repeat it here. This reconstruction is not only high-order accurate in the smooth regions but also essentially non-oscillatory adjacent to the discontinuities. Compared with the standard WENO schemes, the stencils in the reconstruction are more compact.

In addition, we need to reconstruct the point value of $q(x_*, t^n)$, where $q = \phi_x, \phi_{xx}$, and ϕ_{xxx} . The reconstruction procedures of $\phi_x(x_*, t^n), \phi_{xx}(x_*, t^n)$ are the same as those in [33]. For the reconstruction of $\phi_{xxx}(x_*, t^n)$, our numerical experiments show that the following linear reconstruction from $\{\bar{\phi}_i, \bar{v}_i\}_i$ is sufficient to provide an accurate and stable way to approximate $\phi_{xxx}(x_*)$. Let the quintic Hermite polynomial $Q(x)$ satisfy the following condition:

$$\frac{1}{\Delta x} \int_{I_{i+j}} Q(x) dx = \bar{\phi}_{i+j}, \quad \frac{1}{\Delta x} \int_{I_{i+j}} Q(x) \frac{x-x_{i+j}}{\Delta x} dx = \bar{v}_{i+j}, \quad j = -1, 0, 1.$$

Then the values of $\phi_{xxx}(x_*)$ are approximated by:

$$\begin{aligned} \phi_{xxx}(x^1) &\approx Q'''(x^1) = \frac{1}{36\Delta x^3} \left[(445 - 264\sqrt{5})\bar{\phi}_{i-1} + (-540 + 108\sqrt{5})\bar{\phi}_i \right. \\ &\quad \left. + (95 + 156\sqrt{5})\bar{\phi}_{i+1} + (2822 - 1248\sqrt{5})\bar{v}_{i-1} \right. \\ &\quad \left. + (1796 - 3192\sqrt{5})\bar{v}_i + (-418 - 600\sqrt{5})\bar{v}_{i+1} \right], \\ \phi_{xxx}(x^2) &\approx Q'''(x^2) = -\frac{5}{36\Delta x^3} (91\bar{\phi}_{i-1} - 91\bar{\phi}_{i+1} + 314\bar{v}_{i-1} + 1556\bar{v}_i + 314\bar{v}_{i+1}), \\ \phi_{xxx}(x^3) &\approx Q'''(x^3) = -\frac{1}{36\Delta x^3} \left[(95 + 156\sqrt{5})\bar{\phi}_{i-1} + (-540 + 108\sqrt{5})\bar{\phi}_i \right. \\ &\quad \left. + (445 - 264\sqrt{5})\bar{\phi}_{i+1} + (418 + 600\sqrt{5})\bar{v}_{i-1} \right. \\ &\quad \left. + (-1796 + 3192\sqrt{5})\bar{v}_i + (-2822 + 1248\sqrt{5})\bar{v}_{i+1} \right], \end{aligned}$$

where

$$x^1 = x_{i-\frac{1}{2}+\frac{\sqrt{5}}{10}}, \quad x^2 = x_i, \quad x^3 = x_{i+\frac{1}{2}-\frac{\sqrt{5}}{10}}.$$

Remark 1 Following the current central scheme framework, in the Eqs. 2.9 and 2.10 to update $\bar{\phi}_{i+1/2}^{n+1}$ and $\bar{v}_{i+1/2}^{n+1}$, the Hamiltonian functions F are evaluated at x_* with $x_* \in \mathcal{G}^{x,i}$ and the time t^n . This requires the reconstructions of the point values of $\phi_x, \phi_{xx}, \phi_{xxx}$ at x_* based on moments $\{\bar{\phi}_i^n, \bar{v}_i^n\}_i$ at the same time level. Since all the related reconstructions involve stencils including the cell I_i , and x_* are interior points, these reconstructed point values are naturally single-valued. Therefore unlike in upwind type methods, there is no need to use numerical Hamiltonian for F .

2.2 Two-dimensional case

Consider the two-dimensional Hamilton-Jacobi equation

$$\begin{cases} \phi_t + H(\phi_x, \phi_y) = 0, \\ \phi(x, y, 0) = \phi_0(x, y). \end{cases} \tag{2.13}$$

The proposed numerical method will be defined on staggered meshes. For simplicity of presentation, uniform meshes are used with the meshsizes Δx in the x direction, and Δy in the y direction. Each cell of the *primal* mesh is denoted as $I_{ij} = [x_{i-1/2}, x_{i+1/2}] \times [y_{j-1/2}, y_{j+1/2}]$ with its cell center (x_i, y_j) ; and each cell of the *dual* mesh is denoted as $I_{i+1/2, j+1/2} = [x_i, x_{i+1}] \times [y_j, y_{j+1}]$ with its cell center $(x_{i+1/2}, y_{j+1/2})$.

We multiply $\frac{x-x_c}{\Delta x}$, $\frac{y-y_c}{\Delta y}$, and $\frac{x-x_c}{\Delta x} \frac{y-y_c}{\Delta y}$, which are locally scaled linearly independent polynomials of *total* degree one, to Eq. 2.13, and obtain the relations for the first-order moments of the solution

$$\begin{aligned} \phi_t \frac{x-x_c}{\Delta x} + H(\phi_x, \phi_y) \frac{x-x_c}{\Delta x} &= 0, \\ \phi_t \frac{y-y_c}{\Delta y} + H(\phi_x, \phi_y) \frac{y-y_c}{\Delta y} &= 0, \\ \phi_t \frac{x-x_c}{\Delta x} \frac{y-y_c}{\Delta y} + H(\phi_x, \phi_y) \frac{x-x_c}{\Delta x} \frac{y-y_c}{\Delta y} &= 0, \end{aligned} \tag{2.14}$$

where (x_c, y_c) is the center of the relevant mesh element. In particular, for a cell from the primal mesh, we will take $(x_c, y_c) = (x_i, y_j)$ for some i, j ; and for a cell from the dual mesh, we will take $(x_c, y_c) = (x_{i+1/2}, y_{j+1/2})$ for some i, j .

Next we apply the staggered central scheme strategy to Eqs. 2.13 and 2.14 as in one dimension. Suppose at $t = t^n$, the approximations for the zeroth-order and the first-order moments of the solution, denoted as $\{\bar{\phi}_{ij}^n\}_{ij}$, $\{\bar{v}_{ij}^n\}_{ij}$, $\{\bar{w}_{ij}^n\}_{ij}$ and $\{\bar{vw}_{ij}^n\}_{ij}$, are available on the primal mesh, that is, $\forall i, j$,

$$\begin{aligned} \bar{\phi}_{ij}^n &\approx \frac{1}{\Delta x \Delta y} \int_{I_{ij}} \phi(x, y, t^n) dx dy, & \bar{v}_{ij}^n &\approx \frac{1}{\Delta x \Delta y} \int_{I_{ij}} \phi(x, y, t^n) \frac{x-x_i}{\Delta x} dx dy, \\ \bar{w}_{ij}^n &\approx \frac{1}{\Delta x \Delta y} \int_{I_{ij}} \phi(x, y, t^n) \frac{y-y_j}{\Delta y} dx dy, \\ \bar{vw}_{ij}^n &\approx \frac{1}{\Delta x \Delta y} \int_{I_{ij}} \phi(x, y, t^n) \frac{x-x_i}{\Delta x} \frac{y-y_j}{\Delta y} dx dy. \end{aligned}$$

(b.1) We integrate (2.13) and (2.14) over $[t^n, t^{n+1}] \times [x_i, x_{i+1}] \times [y_j, y_{j+1}]$, and approximate all the zeroth-order and the first-order moments of the solution associated with the dual mesh at $t^{n+1} = t^n + \Delta t$, denoted as $\bar{\phi}_{i+1/2, j+1/2}^{n+1}$, $\bar{v}_{i+1/2, j+1/2}^{n+1}$, $\bar{w}_{i+1/2, j+1/2}^{n+1}$ and $\bar{vw}_{i+1/2, j+1/2}^{n+1}$, as follows,

$$\begin{aligned} \bar{\phi}_{i+1/2, j+1/2}^{n+1} &= \bar{\phi}_{i+1/2, j+1/2}^n \\ &\quad - \frac{1}{\Delta x \Delta y} \int_{t^n}^{t^{n+1}} \int_{x_i}^{x_{i+1}} \int_{y_j}^{y_{j+1}} H(\phi_x(x, y, t), \phi_y(x, y, t)) dx dy dt, \end{aligned} \tag{2.15}$$

$$\begin{aligned} \bar{v}_{i+1/2,j+1/2}^{n+1} &= \bar{v}_{i+1/2,j+1/2}^n \\ &\quad - \frac{1}{\Delta x \Delta y} \int_{t^n}^{t^{n+1}} \int_{x_i}^{x_{i+1}} \int_{y_j}^{y_{j+1}} H(\phi_x(x, y, t), \phi_y(x, y, t)) \\ &\quad \times \frac{x - x_{i+1/2}}{\Delta x} dx dy dt, \end{aligned} \tag{2.16}$$

$$\begin{aligned} \bar{w}_{i+1/2,j+1/2}^{n+1} &= \bar{w}_{i+1/2,j+1/2}^n \\ &\quad - \frac{1}{\Delta x \Delta y} \int_{t^n}^{t^{n+1}} \int_{x_i}^{x_{i+1}} \int_{y_j}^{y_{j+1}} H(\phi_x(x, y, t), \phi_y(x, y, t)) \\ &\quad \times \frac{y - y_{j+1/2}}{\Delta y} dx dy dt, \end{aligned} \tag{2.17}$$

$$\begin{aligned} \bar{vw}_{i+1/2,j+1/2}^{n+1} &= \bar{vw}_{i+1/2,j+1/2}^n \\ &\quad - \frac{1}{\Delta x \Delta y} \int_{t^n}^{t^{n+1}} \int_{x_i}^{x_{i+1}} \int_{y_j}^{y_{j+1}} H(\phi_x(x, y, t), \phi_y(x, y, t)) \\ &\quad \times \frac{x - x_{i+1/2}}{\Delta x} \frac{y - y_{j+1/2}}{\Delta y} dx dy dt. \end{aligned} \tag{2.18}$$

All the terms on the right-hand side of Eqs. 2.15–2.18 will be reconstructed based on $\{\bar{\phi}_{ij}^n, \bar{v}_{ij}^n, \bar{w}_{ij}^n, \bar{vw}_{ij}^n\}_{ij}$. For simplicity of notation, we still use ϕ in the above formulations, though it is no longer the exact solution.

- (b.2) We then integrate Eqs. 2.13 and 2.14 over $[t^{n+1}, t^{n+2}] \times [x_{i-1/2}, x_{i+1/2}] \times [y_{j-1/2}, y_{j+1/2}]$, and approximate the moments of the solution with respect to the primal mesh at $t^{n+2} = t^{n+1} + \Delta t$,

$$\begin{aligned} \bar{\phi}_{ij}^{n+2} &= \bar{\phi}_{ij}^{n+1} - \frac{1}{\Delta x \Delta y} \int_{t^{n+1}}^{t^{n+2}} \int_{x_{i-1/2}}^{x_{i+1/2}} \int_{y_{j-1/2}}^{y_{j+1/2}} H(\phi_x(x, y, t), \\ &\quad \phi_y(x, y, t)) dx dy dt, \\ \bar{v}_{ij}^{n+2} &= \bar{v}_{ij}^{n+1} - \frac{1}{\Delta x \Delta y} \int_{t^{n+1}}^{t^{n+2}} \int_{x_{i-1/2}}^{x_{i+1/2}} \int_{y_{j-1/2}}^{y_{j+1/2}} H(\phi_x(x, y, t), \\ &\quad \phi_y(x, y, t)) \frac{x - x_i}{\Delta x} dx dy dt, \\ \bar{w}_{ij}^{n+2} &= \bar{w}_{ij}^{n+1} - \frac{1}{\Delta x \Delta y} \int_{t^{n+1}}^{t^{n+2}} \int_{x_{i-1/2}}^{x_{i+1/2}} \int_{y_{j-1/2}}^{y_{j+1/2}} H(\phi_x(x, y, t), \\ &\quad \phi_y(x, y, t)) \frac{y - y_j}{\Delta y} dx dy dt, \\ \bar{vw}_{ij}^{n+2} &= \bar{vw}_{ij}^{n+1} - \frac{1}{\Delta x \Delta y} \int_{t^{n+1}}^{t^{n+2}} \int_{x_{i-1/2}}^{x_{i+1/2}} \int_{y_{j-1/2}}^{y_{j+1/2}} H(\phi_x(x, y, t), \\ &\quad \phi_y(x, y, t)) \frac{x - x_i}{\Delta x} \frac{y - y_j}{\Delta y} dx dy dt. \end{aligned}$$

- (b.3) Set n to be $n + 2$, and go to (b.1).

Note that the mesh switches back after two time steps.

From now on, we will focus on the update details from t^n to t^{n+1} . Since our spatial reconstructions are fifth-order, we further approximate all the spatial integrals

in Eqs. 2.15–2.18 with the four-point Gauss-Lobatto quadrature formula along each direction,

$$\begin{aligned} \bar{\phi}_{i+1/2,j+1/2}^{n+1} &= \bar{\phi}_{i+1/2,j+1/2}^n - \sum_{l=1}^4 \sum_{s=1}^4 \omega_l \omega_s \\ &\int_{t^n}^{t^{n+1}} H(\phi_x(\mathcal{G}_l^x, \mathcal{G}_s^y, t), \phi_y(\mathcal{G}_l^x, \mathcal{G}_s^y, t)) dt, \end{aligned} \tag{2.19}$$

$$\begin{aligned} \bar{v}_{i+1/2,j+1/2}^{n+1} &= \bar{v}_{i+1/2,j+1/2}^n - \sum_{l=1}^4 \sum_{s=1}^4 \omega_l \omega_s \frac{\mathcal{G}_l^x - x_{i+1/2}}{\Delta x} \\ &\int_{t^n}^{t^{n+1}} H(\phi_x(\mathcal{G}_l^x, \mathcal{G}_s^y, t), \phi_y(\mathcal{G}_l^x, \mathcal{G}_s^y, t)) dt, \end{aligned} \tag{2.20}$$

$$\begin{aligned} \bar{w}_{i+1/2,j+1/2}^{n+1} &= \bar{w}_{i+1/2,j+1/2}^n - \sum_{l=1}^4 \sum_{s=1}^4 \omega_l \omega_s \frac{\mathcal{G}_s^y - y_{j+1/2}}{\Delta y} \\ &\int_{t^n}^{t^{n+1}} H(\phi_x(\mathcal{G}_l^x, \mathcal{G}_s^y, t), \phi_y(\mathcal{G}_l^x, \mathcal{G}_s^y, t)) dt, \end{aligned} \tag{2.21}$$

$$\begin{aligned} \bar{v}\bar{w}_{i+1/2,j+1/2}^{n+1} &= \bar{v}\bar{w}_{i+1/2,j+1/2}^n \\ &- \sum_{l=1}^4 \sum_{s=1}^4 \omega_l \omega_s \frac{\mathcal{G}_l^x - x_{i+1/2}}{\Delta x} \frac{\mathcal{G}_s^y - y_{j+1/2}}{\Delta y} \\ &\int_{t^n}^{t^{n+1}} H(\phi_x(\mathcal{G}_l^x, \mathcal{G}_s^y, t), \phi_y(\mathcal{G}_l^x, \mathcal{G}_s^y, t)) dt. \end{aligned} \tag{2.22}$$

where $\{\omega_l\}_{l=1}^4$ and $\{\mathcal{G}_l^x\}_{l=1}^4$ are given in Section 2.1, and $\{\mathcal{G}_s^y\}_{s=1}^4$ are Gauss-Lobatto quadrature points over the cell $[y_j, y_{j+1}]$

$$\mathcal{G}_1^y = y_j, \quad \mathcal{G}_2^y = y_{j+\frac{1}{2}-\frac{\sqrt{5}}{10}}, \quad \mathcal{G}_3^y = y_{j+\frac{1}{2}+\frac{\sqrt{5}}{10}}, \quad \mathcal{G}_4^y = y_{j+1}.$$

For the primal mesh I_{ij} , the collection of such quadrature points is denoted as

$$\mathcal{G} = \left\{ (x, y) : x \in \mathcal{G}^{x,i}, y \in \mathcal{G}^{y,j}, \forall i, j \right\}, \tag{2.23}$$

where $\mathcal{G}^{x,i}$ is given in Section 2.1, and $\mathcal{G}^{y,j} = \{y_{j-\frac{1}{2}+\frac{\sqrt{5}}{10}}, y_j, y_{j+\frac{1}{2}-\frac{\sqrt{5}}{10}}\}$.

Suppose the solution at t^n is piecewise constant with respect to the primal mesh, and the time step Δt is chosen to satisfy the CFL restriction $\Delta t \leq \frac{C_{cfl}}{(\max_{i,j} |H_1(x_i, y_j, t^n)| / \Delta x + \max_{i,j} |H_2(x_i, y_j, t^n)| / \Delta y)}$ with some constant C_{cfl} and $(H_1(x_i, y_j, t^n), H_2(x_i, y_j, t^n))$ defined below (2.29) being related to the characteristic speed of Eq. 2.13, one can expect the solution restricted at $(x_*, y_*) \in \mathcal{G}$ are smooth with respect to $t \in [t^n, t^{n+1}]$. Under such assumption on the time step, the

Hamiltonian function $H(\phi_x(x_*, y_*, t), \phi_y(x_*, y_*, t))$ in Eqs. 2.19–2.22 can be approximated by a temporal Taylor expansion at t^n according to the following

$$\begin{aligned}
 H(\phi_x(x_*, y_*, t), \phi_y(x_*, y_*, t)) &\approx H(\phi_x(x_*, y_*, t^n), \phi_y(x_*, y_*, t^n)) \\
 &+ (t - t^n) \frac{\partial}{\partial t} H(\phi_x(x_*, y_*, t^n), \phi_y(x_*, y_*, t^n)) \\
 &+ \frac{(t - t^n)^2}{2} \frac{\partial^2}{\partial t^2} H(\phi_x(x_*, y_*, t^n), \phi_y(x_*, y_*, t^n)).
 \end{aligned}
 \tag{2.24}$$

If we want to obtain the $(k + 1)$ th-order accuracy in time, we need to approximate the first k time derivatives of H . Just as in one-dimensional case, we here only consider a third-order discretization in time.

Plugging the relations (2.24) into Eqs. 2.19–2.22, this will lead to our actual update formulations

$$\bar{\phi}_{i+1/2, j+1/2}^{n+1} = \bar{\phi}_{i+1/2, j+1/2}^n - \sum_{l=1}^4 \sum_{s=1}^4 \omega_l \omega_s F(\phi(\mathcal{G}_l^x, \mathcal{G}_s^y, t^n)),
 \tag{2.25}$$

$$\bar{v}_{i+1/2, j+1/2}^{n+1} = \bar{v}_{i+1/2, j+1/2}^n - \sum_{l=1}^4 \sum_{s=1}^4 \omega_l \omega_s \frac{\mathcal{G}_l^x - x_{i+1/2}}{\Delta x} F(\phi(\mathcal{G}_l^x, \mathcal{G}_s^y, t^n)),
 \tag{2.26}$$

$$\bar{w}_{i+1/2, j+1/2}^{n+1} = \bar{w}_{i+1/2, j+1/2}^n - \sum_{l=1}^4 \sum_{s=1}^4 \omega_l \omega_s \frac{\mathcal{G}_s^y - y_{j+1/2}}{\Delta y} F(\phi(\mathcal{G}_l^x, \mathcal{G}_s^y, t^n)),
 \tag{2.27}$$

$$\begin{aligned}
 \bar{v}\bar{w}_{i+1/2, j+1/2}^{n+1} &= \bar{v}\bar{w}_{i+1/2, j+1/2}^n - \sum_{l=1}^4 \sum_{s=1}^4 \omega_l \omega_s \frac{\mathcal{G}_l^x - x_{i+1/2}}{\Delta x} \frac{\mathcal{G}_s^y - y_{j+1/2}}{\Delta y} \\
 &F(\phi(\mathcal{G}_l^x, \mathcal{G}_s^y, t^n)).
 \end{aligned}
 \tag{2.28}$$

with

$$\begin{aligned}
 F &= F(\phi) = \Delta t H + \frac{\Delta t^2}{2} \frac{\partial}{\partial t} H + \frac{\Delta t^3}{6} \frac{\partial^2}{\partial t^2} H \\
 &= \Delta t H + \frac{\Delta t^2}{2} (H_1 \phi_{xt} + H_2 \phi_{yt}) \\
 &\quad + \frac{\Delta t^3}{6} (H_{11} \phi_{xt}^2 + 2H_{12} \phi_{xt} \phi_{yt} + H_{22} \phi_{yt}^2 + H_1 \phi_{xtt} + H_2 \phi_{ytt}).
 \end{aligned}
 \tag{2.29}$$

where H_i is the partial derivative of the Hamiltonian H with respect to i th argument and H_{ij} is the second partial derivative of H with respect to i th and j th arguments.

Again, we convert the temporal derivative terms of ϕ in Eq. 2.29 into spatial ones by repeatedly using the governing equation (2.13):

$$\begin{aligned}
 \phi_{xt} &= -H_1 \phi_{xx} - H_2 \phi_{xy}, \quad \phi_{yt} = -H_1 \phi_{xy} - H_2 \phi_{yy}, \\
 \phi_{xtt} &= (H_1^2 \phi_{xx} + 2H_1 H_2 \phi_{xy} + H_2^2 \phi_{yy})_x \\
 &= 2H_1 H_{11} \phi_{xx}^2 + 2H_1 H_{12} \phi_{xy} \phi_{xx} + H_1^2 \phi_{xxx} \\
 &\quad + 2\phi_{xy} [(H_{11} \phi_{xx} + H_{12} \phi_{xy}) H_2 + (H_{21} \phi_{xx} + H_{22} \phi_{xy}) H_1] + 2H_1 H_2 \phi_{xxy} \\
 &\quad + 2H_2 H_{21} \phi_{xx} \phi_{yy} + 2H_2 H_{22} \phi_{xy} \phi_{yy} + H_2^2 \phi_{yyy}, \\
 \phi_{ytt} &= (H_1^2 \phi_{xx} + 2H_1 H_2 \phi_{xy} + H_2^2 \phi_{yy})_y \\
 &= 2H_1 H_{11} \phi_{xx} \phi_{xy} + 2H_1 H_{12} \phi_{xx} \phi_{yy} + H_1^2 \phi_{xxy} \\
 &\quad + 2\phi_{xy} [(H_{11} \phi_{xy} + H_{12} \phi_{yy}) H_2 + (H_{21} \phi_{xy} + H_{22} \phi_{yy}) H_1] + 2H_1 H_2 \phi_{xyy} \\
 &\quad + 2H_2 H_{21} \phi_{xy} \phi_{yy} + 2H_2 H_{22} \phi_{yy}^2 + H_2^2 \phi_{yyy},
 \end{aligned}
 \tag{2.30}$$

Even though $F(\phi)$ is used throughout the presentation, one should keep in mind that we indeed have $F = \mathcal{F}(\phi_x, \phi_y, \phi_{xx}, \phi_{xy}, \phi_{yy}, \phi_{xxx}, \phi_{xxy}, \phi_{xyy}, \phi_{yyy})$.

To obtain the moments $\bar{\phi}_{i+1/2,j+1/2}^{n+1}, \bar{v}_{i+1/2,j+1/2}^{n+1}, \bar{w}_{i+1/2,j+1/2}^{n+1}$ and $\bar{vw}_{i+1/2,j+1/2}^{n+1}$ on the dual mesh at the next time t^{n+1} based on Eqs. 2.25–2.28, one will need to reconstruct at the current time $t^n, \forall i, j$,

- (1) the moments $\bar{\phi}_{i+1/2,j+1/2}^n, \bar{v}_{i+1/2,j+1/2}^n, \bar{w}_{i+1/2,j+1/2}^n$ and $\bar{vw}_{i+1/2,j+1/2}^n$ on the dual mesh, as well as
- (2) the point value of $q(x_*, y_*, t^n)$, where $q = \phi_x, \phi_y, \phi_{xx}, \phi_{xy}, \phi_{yy}, \phi_{xxx}, \phi_{xxy}, \phi_{xyy}$, or ϕ_{yyy} , and they are the function F in Eq. 2.29 actually depends on. Here $(x_*, y_*) \in \mathcal{G}$.

Just as in one dimension, to obtain the cell average $\bar{\phi}_{i+1/2,j+1/2}^n, \forall i, j$, one would want to get the following four quarter-cell averages

$$\begin{aligned} & \frac{1}{\Delta x \Delta y} \int_{x_i}^{x_{i+1/2}} \int_{y_j}^{y_{j+1/2}} \phi(x, y, t^n) dx dy, & \frac{1}{\Delta x \Delta y} \int_{x_{i+1/2}}^{x_{i+1}} \int_{y_j}^{y_{j+1/2}} \phi(x, y, t^n) dx dy, \\ & \frac{1}{\Delta x \Delta y} \int_{x_i}^{x_{i+1/2}} \int_{y_{j+1/2}}^{y_{j+1}} \phi(x, y, t^n) dx dy, & \frac{1}{\Delta x \Delta y} \int_{x_{i+1/2}}^{x_{i+1}} \int_{y_{j+1/2}}^{y_{j+1}} \phi(x, y, t^n) dx dy. \end{aligned} \tag{2.31}$$

This similarly goes to all the first-order moments.

To reconstruct the quarter-cell moments and point values mentioned above, we use a dimension-by-dimension procedure and apply the one-dimensional fifth-order accurate HWENO reconstruction in [33] and linear reconstruction for ϕ_{xxx} in Section 2.1 multiple times. The dimension-by-dimension reconstruction greatly improves the computational efficiency and ease of the implementation of high dimensional cases. Such treatment is possible in our proposed work mainly due to the inclusion of the mixed first-order moment \bar{vw}_{ij}^n .

We adopt the same reconstruction of the quarter-cell moments as in [33] and we will not repeat it here. The difference between [33] and this paper is that in [33] we need to reconstruct the point value of $q(x_*, y_*, t^n)$, where $q = u, u_x, u_y, u_{xx}, u_{xy}$ or u_{yy} and u is the solution of hyperbolic conservation laws. However, we need to reconstruct the point value of $q(x_*, y_*, t^n)$, where $q = \phi_x, \phi_y, \phi_{xx}, \phi_{xy}, \phi_{yy}, \phi_{xxx}, \phi_{xxy}, \phi_{xyy}$, or ϕ_{yyy} in this paper. We will describe the reconstruction of point values of the derivatives of the solution briefly. It is based on the moments $\{\bar{\phi}_{ij}^n, \bar{v}_{ij}^n, \bar{w}_{ij}^n, \bar{vw}_{ij}^n\}_{ij}$ on the primal mesh at $t = t^n$. The superscript n will be omitted, together with the dependence on the time t .

Step 1. Along x direction, based on $\{\bar{\phi}_{ij}, \bar{v}_{ij}\}_{ij}$, we reconstruct

$$\frac{1}{\Delta y} \int_{y_{j-1/2}}^{y_{j+1/2}} p(x_*, y) dy, \quad p = \phi, \phi_x, \phi_{xx}, \phi_{xxx}, \quad x_* \in \mathcal{G}^{x,i}.$$

Step 2. Along x direction, based on $\{\bar{w}_{ij}, \bar{vw}_{ij}\}_{ij}$, we reconstruct

$$\frac{1}{\Delta y} \int_{y_{j-1/2}}^{y_{j+1/2}} p(x_*, y) \frac{y - y_j}{\Delta y} dy, \quad p = \phi, \phi_x, \phi_{xx}, \phi_{xxx}, \quad x_* \in \mathcal{G}^{x,i}.$$

Step 3. Along y direction, based on

$$\frac{1}{\Delta y} \int_{y_{j-1/2}}^{y_{j+1/2}} p(x_*, y) dy, \quad \frac{1}{\Delta y} \int_{y_{j-1/2}}^{y_{j+1/2}} p(x_*, y) \frac{y - y_j}{\Delta y} dy,$$

$$p = \phi, \phi_x, \phi_{xx}, \phi_{xxx}, \quad x_* \in \mathcal{G}^{x,i}$$

with all i, j , we reconstruct

$$q(x_*, y_*), \quad q = \phi_x, \phi_y, \phi_{xx}, \phi_{xy}, \phi_{yy}, \phi_{xxx}, \phi_{xxy}, \phi_{xyy}, \phi_{yyy}, \quad (x_*, y_*) \in \mathcal{G}.$$

Remark 2 Similar as in the one-dimensional case (see also Remark 1), with the current central scheme framework, there is no need to use numerical Hamiltonian for F as in upwind type schemes.

3 Central Hermite WENO schemes with natural continuous extension of Runge-Kutta time discretization

Alternative to the Lax-Wendroff strategy, we apply in this section the natural continuous extension of Runge-Kutta (NCE-RK) time discretizations, to combine with the central HWENO spatial discretizations in the framework of staggered meshes. The use of NCE-RK methods permits one to compute accurate approximations for the intermediate value of a solution to an ODE based on standard RK methods with slight increase of the computational cost. Note that a standard RK method in general only provides accurate approximations for the solution at discrete time t^n for any n .

Below we will describe a fourth-order NCE-RK method which is used in this paper. For more details about such time discretizations, one can refer to [3, 35]. Consider an ODE problem

$$\begin{cases} y'(t) = F(t, y(t)), \\ y(t_0) = y_0, \end{cases} \tag{3.1}$$

and suppose y^n is a given approximation to $y(t^n)$. One can then approximate $y(t^{n+1})$ at $t^{n+1} = t^n + \Delta t$ by y^{n+1} with a standard four-stage fourth-order RK scheme as follows.

$$y^{n+1} = y^n + \Delta t \sum_{i=1}^4 b_i K^{(i)}, \tag{3.2}$$

where $K^{(i)}$ is an RK flux determined by

$$K^{(i)} = F(t^n + c_i \Delta t, Y^{(i)}) \quad \text{with } Y^{(i)} = y^n + c_i \Delta t K^{(i-1)}, \quad i = 1, 2, 3, 4, \tag{3.3}$$

and $K^{(0)} = 0$. In addition, $b_1 = b_4 = \frac{1}{6}$, $b_2 = b_3 = \frac{1}{3}$, and $c_1 = 0, c_2 = c_3 = \frac{1}{2}, c_4 = 1$.

A natural continuous extension of the RK scheme (3.2)–(3.3) further provides an approximation of $y(t)$ (and also its derivatives) with the same accuracy when $t \in [t^n, t^{n+1}]$. This approximation is given specifically by

$$s(t)|_{t=t^n+\theta\Delta t} := y^n + \Delta t \sum_{i=1}^4 B_i(\theta)K^{(i)}, \quad 0 \leq \theta \leq 1,$$

where

$$\begin{aligned} B_1(\theta) &= 2(1 - 4b_1)\theta^3 + 3(3b_1 - 1)\theta^2 + \theta, \\ B_i(\theta) &= 4(3c_i - 2)b_i\theta^3 + 3(3 - 4c_i)b_i\theta^2, \quad i = 2, 3, 4. \end{aligned}$$

$s(t)$ not only satisfies $s(t^n) = y^n$, $s(t^{n+1}) = y^{n+1}$, but also has the following approximation properties,

$$\max_{t^n \leq t \leq t^{n+1}} |y^{(l)}(t) - s^{(l)}(t)| = O(\Delta t^{4-l}), \quad 0 \leq l \leq 4.$$

3.1 One-dimensional case

We use the same notation for the staggered meshes and the moments of a function as in Section 2.1. Though the discussion below focuses on one time step, one would want to keep in mind that the overall algorithm is still based on staggered meshes, and it switches back and forth between the primal and dual meshes.

Suppose at $t = t^n$, the approximations for the moments of the solution, namely $\{\bar{\phi}_i^n\}_i$ and $\{\bar{v}_i^n\}_i$, are available on the primal mesh.

We start our scheme based on Eqs. 2.5 and 2.6. As discussed in Section 2.1, if the time step Δt is chosen to satisfy a CFL restriction $\Delta t \leq \frac{C_{cfl}\Delta x}{\max_i |H'(\phi_x(x_i, t^n))|}$ with some constant C_{cfl} , the solution of this problem restricted at x_* with $x_* \in \mathcal{G}^{x,i}, \forall i$ are smooth for $t \in [t^n, t^{n+1}]$. Motivated by this, the temporal Hamiltonian integrals in the right of Eqs. 2.5–2.6 involve only smooth integrands and can be evaluated by numerical quadrature with compatible accuracy. We apply the three-point Gaussian quadrature formula and replace the temporal integral terms in Eqs. 2.5–2.6 according to the following

$$\int_{t^n}^{t^{n+1}} H(\phi_x(x_*, t))dt \approx \Delta t \sum_{l=1}^3 \alpha_l H(\phi_x(x_*, t^n + \Delta t\theta_l)). \tag{3.4}$$

Here $\alpha_1 = \alpha_3 = \frac{5}{18}, \alpha_2 = \frac{4}{9}$ are the quadrature weights, and $\theta_1 = \frac{1}{2} - \frac{\sqrt{15}}{10}, \theta_2 = \frac{1}{2}, \theta_3 = \frac{1}{2} + \frac{\sqrt{15}}{10}$ are the quadrature points.

Based on Eqs. 2.5–2.6 and 3.4, one can compute the moments of the solution, namely $\{\bar{\phi}_{i+1/2}^{n+1}\}_i$ and $\{\bar{v}_{i+1/2}^{n+1}\}_i$, with respect to the dual mesh at $t = t^{n+1}$. To achieve this, one only needs to obtain accurate approximations for

$$\bar{\phi}_{i+1/2}^n, \bar{v}_{i+1/2}^n, \phi_x(x_*, t^n + \Delta t\theta_l), l = 1, 2, 3, x_* \in \mathcal{G}^{x,i}, \forall i, \tag{3.5}$$

and the remainder of this subsection will be devoted to the related details.

Recall at t^n , $\{\bar{\phi}_i^n, \bar{v}_i^n\}_i$ are available. We can first reconstruct the staggered moments $\{\bar{\phi}_{i+1/2}^n\}_i$ and $\{\bar{v}_{i+1/2}^n\}_i$ associated with the dual mesh in Eq. 3.5 based on the same fifth-order HWENO procedure as in Section 2.1.

In order to approximate the point values $\phi_x(x_*, t^n + \Delta t\theta_l), l = 1, 2, 3, x_* \in \mathcal{G}^{x,i}, \forall i$ in Eq. 3.5, we will apply the fourth-order NCE-RK method to the auxiliary ODE problem (3.1) starting from $t = t^n$ at each $x_* \in \mathcal{G}^{x,i}$, with any i , where

$$y(t) = \phi_x(x_*, t), \quad F(t, y) = -H_x(\phi_x)|_{(x_*,t)} \approx -\mathcal{R}_{H_x}(\phi_x)|_{(x_*,t)}. \quad (3.6)$$

Here the operator \mathcal{R}_{H_x} in Eq. 3.6 is to reconstruct H_x at x_* , which can be computed by the same WENO strategy as f_x in [33].

More specifically, one needs to evaluate the corresponding $K^{(i)}, i = 1, 2, 3, 4$, used in Eqs. 3.2–3.3 as follows.

- (c.1) To evaluate $K^{(1)}$, we reconstruct the point values of $\phi_x(x_*, t^n)$ based on the given moments $\{\overline{\phi}_i^n, \overline{v}_i^n\}_i$ on the primal mesh which has already been discussed in [33]. The operator \mathcal{R}_{H_x} is chosen such that $H_x(x_*, t^n)$ is reconstructed by a WENO strategy used in [33].
- (c.2) Once $K^{(l)}$ for some $l \geq 1$ is available, then $Y^{(l+1)}$ can be computed based on Eq. 3.3. This will provide approximations for $\phi_x(x_*, t^n + c_{l+1}\Delta t)$. Now the operator \mathcal{R}_{H_x} in Eq. 3.6 is chosen such that $H_x(x_*, t^n + c_{l+1}\Delta t)$ is reconstructed using a WENO strategy.
- (c.3) With $K^{(l)}, l = 1, 2, 3, 4$, one can now follow the NCE-RK procedure to obtain accurate approximations for the point values of ϕ_x in Eq. 3.5.

3.2 Two-dimensional case

We use the same notation for the staggered meshes and the moments of a function, as well as the fifth-order HWENO spatial reconstruction as in Section 2.2. Again, the discussion will focus on the algorithm over one time step.

Suppose at $t = t^n$, the approximations for the moments of the solution, namely $\{\overline{\phi}_{ij}^n, \overline{v}_{ij}^n, \overline{w}_{ij}^n, \overline{vw}_{ij}^n\}_{ij}$, are available on the primal mesh. We start the two-dimensional case based on Eqs. 2.19–2.22. Following the idea in Section 2.2, if the time step Δt is chosen to satisfy the CFL restriction $\Delta t \leq \frac{C_{cfl}}{(\max_{i,j} |H_1(x_i, y_j, t^n)|/\Delta x + \max_{i,j} |H_2(x_i, y_j, t^n)|/\Delta y)}$ with some constant C_{cfl} , one can expect the solution restricted at $(x_*, y_*) \in \mathcal{G}$ are smooth with respect to $t \in [t^n, t^{n+1}]$. Under such assumption on the time step, we further apply the three-point Gaussian quadrature formula and replace the temporal integral terms in Eqs. 2.19–2.22 according to the following numerical quadrature

$$\int_{t^n}^{t^{n+1}} H(\phi_x(x_*, y_*, t), \phi_y(x_*, y_*, t))dt \approx \Delta t \sum_{l=1}^3 \alpha_l H(\phi_x(x_*, y_*, t^n + \Delta t\theta_l), \phi_y(x_*, y_*, t^n + \Delta t\theta_l)), \quad (3.7)$$

where $\alpha_1 = \alpha_3 = \frac{5}{18}, \alpha_2 = \frac{4}{9}$, and $\theta_1 = \frac{1}{2} - \frac{\sqrt{15}}{10}, \theta_2 = \frac{1}{2}, \theta_3 = \frac{1}{2} + \frac{\sqrt{15}}{10}$.

Based on Eqs. 2.19–2.22 and 3.7, one can compute the moments of the solution, namely

$$\{\overline{\phi}_{i+1/2, j+1/2}^{n+1}, \overline{v}_{i+1/2, j+1/2}^{n+1}, \overline{w}_{i+1/2, j+1/2}^{n+1}, \overline{vw}_{i+1/2, j+1/2}^{n+1}\}_{ij},$$

associated with the dual mesh at $t = t^{n+1}$. To achieve this, one only needs to obtain accurate approximations for

$$\begin{aligned} \bar{p}_{i+1/2,j+1/2}^n, q(x_*, y_*, t^n + \Delta t\theta_l), \text{ with } p = \phi, v, w, vw, q = \phi_x, \phi_y, \\ \text{and } (x_*, y_*) \in \mathcal{G}, l = 1, 2, 3, \forall i, j \end{aligned} \quad (3.8)$$

and the remainder of this subsection will be devoted to the related details.

Recall at t^n , $\{\bar{\phi}_{ij}^n, \bar{v}_{ij}^n, \bar{w}_{ij}^n, \bar{vw}_{ij}^n\}_{ij}$ are available. We can first reconstruct the staggered moments $\{\bar{\phi}_{i+1/2,j+1/2}^n, \bar{v}_{i+1/2,j+1/2}^n, \bar{w}_{i+1/2,j+1/2}^n, \bar{vw}_{i+1/2,j+1/2}^n\}_{ij}$ in Eq. 3.8 based on the same fifth-order HWENO procedure described in [33]. In order to approximate the point values $q(x_*, y_*, t^n + \Delta t\theta_l)$ with $q = \phi_x, \phi_y, (x_*, y_*) \in \mathcal{G}, l = 1, 2, 3$ in Eq. 3.8, we will apply the fourth-order NCE-RK method to the auxiliary ODE problem (3.1) starting from $t = t^n$ at each (x_*, y_*) , where

$$y(t) = \begin{cases} \phi_x(x_*, y_*, t), \\ \phi_y(x_*, y_*, t), \end{cases} \quad F(t, y) = \begin{cases} -H_x(\phi_x, \phi_y)|_{(x_*, y_*, t)} \approx -\mathcal{R}_{H_x}(\phi_x, \phi_y)|_{(x_*, y_*, t)}, \\ -H_y(\phi_x, \phi_y)|_{(x_*, y_*, t)} \approx -\mathcal{R}_{H_y}(\phi_x, \phi_y)|_{(x_*, y_*, t)}. \end{cases} \quad (3.9)$$

Here the operators \mathcal{R}_{H_x} and \mathcal{R}_{H_y} are to reconstruct H_x and H_y at (x_*, y_*) respectively, and they are evaluated by the same WENO strategy as f_x and g_y in [33].

Then, one can evaluate the corresponding $K^{(i)}, i = 1, 2, 3, 4$ used in Eqs. 3.2-3.3 as follows.

- (d.1) To evaluate $K^{(1)}$, we reconstruct the point values of $q(x_*, y_*, t^n), q = \phi_x, \phi_y$ based on the given moments $\{\bar{\phi}_{ij}^n, \bar{v}_{ij}^n, \bar{w}_{ij}^n, \bar{vw}_{ij}^n\}_{ij}$ on the primal mesh which is used in Section 2.2. The operators \mathcal{R}_{H_x} and \mathcal{R}_{H_y} are chosen such that $H_x(x_*, y_*, t^n)$ and $H_y(x_*, y_*, t^n)$ are reconstructed by the WENO procedure discussed in [33].
- (d.2) Once $K^{(l)}$ for some $l \geq 1$ is available, then $Y^{(l+1)}$ can be computed based on Eq. 3.3. This will provide approximations for $q(x_*, y_*, t^n + c_{l+1}\Delta t), q = \phi_x, \phi_y$. Again, The operators \mathcal{R}_{H_x} and \mathcal{R}_{H_y} are chosen such that $H_x(x_*, y_*, t^n + c_{l+1}\Delta t)$ and $H_y(x_*, y_*, t^n + c_{l+1}\Delta t)$ are reconstructed by the same procedure as in (d.1).
- (d.3) With $K^{(l)}, l = 1, 2, 3, 4$, one can now follow the NCE-RK procedure to obtain accurate approximations for the point values of ϕ_x and ϕ_y in Eq. 3.8.

Remark 3 For the two-dimensional example 4.14 in Section 4, we notice that the Hamiltonian H depends on not only the first derivatives ϕ_x, ϕ_y , but also the second derivatives $\phi_{xx}, \phi_{xy}, \phi_{yy}$. There will be more terms (three two-dimensional second spatial derivatives) for $y(t)$, and three more two-dimensional second derivatives of H for $F(t, y)$ in Eq. 3.9 are needed by the similar reconstruction strategy.

4 Numerical examples

In this section, we will report a set of numerical experiments to illustrate the high-order accuracy and the robustness of the proposed methods to simulate one- and two-dimensional HJ equations (1.1). The solutions can be smooth or have discontinuous

derivative. The numerical results are obtained by the proposed fifth-order central HWENO scheme with the third-order Lax-Wendroff method (C-HWENO5-LW3) or with the fourth-order NCE-RK method (C-HWENO5-NCERK4) in time for both one and two dimensions. Uniform meshes with N elements and $N_x \times N_y$ elements are used in one and two dimensions, respectively.

The time step Δt is dynamically chosen. In particular, in one-dimensional scalar case, we take

$$\Delta t = C_{cfl} \frac{\Delta x}{\max_i |H'(\phi_x(x_i, t))|},$$

and in two-dimensional scalar case, we have

$$\Delta t = \frac{C_{cfl}}{(\max_{i,j} |H_1(x_i, y_j, t)|/\Delta x + \max_{i,j} |H_2(x_i, y_j, t)|/\Delta y)},$$

and they are computed numerically at each discrete time level.

The CFL number C_{cfl} is taken as 0.2 for non-smooth tests. For accuracy test cases, in order to ensure the spatial errors dominate, we should take $\Delta t = O(\Delta x^{5/4})$, for simplicity, we take $C_{cfl} = 0.05$, and this can ensure $\Delta t = O(\Delta x^{5/4})$ for all test cases in this paper.

In addition, the L_1 and L_∞ errors are defined as below. Suppose the final time is T . In one-dimensional case, assuming $x \in [a, b]$ and each cell of the mesh of the form $I_i, i = 1, \dots, N$, we take

$$\begin{aligned} \|e(\cdot, T)\|_{L_1} &= \frac{1}{b-a} \sum_{i=1}^N \left| \bar{\phi}_i(T) - \frac{1}{\Delta x} \int_{I_i} \phi(x, T) dx \right| \Delta x \\ &= \frac{1}{N} \sum_{i=1}^N \left| \bar{\phi}_i(T) - \frac{1}{\Delta x} \int_{I_i} \phi(x, T) dx \right|, \\ \|e(\cdot, T)\|_{L_\infty} &= \max_{1 \leq i \leq N} \left| \bar{\phi}_i(T) - \frac{1}{\Delta x} \int_{I_i} \phi(x, T) dx \right|, \end{aligned}$$

and in two-dimensional case, assuming $x \in [a, b], y \in [c, d]$ and each cell of the mesh of the form $I_{ij}, i = 1, \dots, N_x, j = 1, \dots, N_y$, we have

$$\begin{aligned} \|e(\cdot, \cdot, T)\|_{L_1} &= \frac{1}{(b-a)(d-c)} \sum_{i=1}^{N_x} \sum_{j=1}^{N_y} \left| \bar{\phi}_{ij}(T) - \frac{1}{\Delta x \Delta y} \int_{I_{ij}} \phi(x, y, T) dx dy \right| \Delta x \Delta y \\ &= \frac{1}{N_x N_y} \sum_{i=1}^{N_x} \sum_{j=1}^{N_y} \left| \bar{\phi}_{ij}(T) - \frac{1}{\Delta x \Delta y} \int_{I_{ij}} \phi(x, y, T) dx dy \right|, \\ \|e(\cdot, \cdot, T)\|_{L_\infty} &= \max_{1 \leq i \leq N_x, 1 \leq j \leq N_y} \left| \bar{\phi}_{ij}(T) - \frac{1}{\Delta x \Delta y} \int_{I_{ij}} \phi(x, y, T) dx dy \right|. \end{aligned}$$

4.1 Accuracy tests with smooth solutions

We first test the accuracy of the proposed schemes when the solutions are smooth. The problems can be linear, nonlinear, convex or non-convex in one and two dimensions.

Example 4.1 We consider the one-dimensional linear advection equation,

$$\phi_t + \phi_x = 0 \tag{4.1}$$

with the initial condition $\phi(x, 0) = \sin(\pi x)$, and a 2-periodic boundary condition. The solutions are run up to $t = 2$, i.e. after one period by the schemes. In Table 1 we present the L_1 and L_∞ errors and numerical orders of accuracy for C-HWENO5-LW3 and C-HWENO5-NCERK4 schemes. One can see that both schemes achieve their designed fifth-order accuracy.

Example 4.2 We consider the one-dimensional Burgers equation, which is scalar and nonlinear,

$$\phi_t + \frac{(\phi_x + 1)^2}{2} = 0 \tag{4.2}$$

with the initial condition $\phi(x, 0) = -\cos(\pi x)$, and a 2-periodic boundary condition. When $t = 0.5/\pi^2$ the derivative of solution is still smooth, and the L_1 and L_∞ errors and numerical orders of accuracy are presented in Table 2 for C-HWENO5-LW3 and C-HWENO5-NCERK4 schemes. We can see that both schemes achieve their designed fifth-order accuracy with comparable errors.

Example 4.3 We consider the following nonlinear scalar one-dimensional Hamilton-Jacobi equation

$$\phi_t - \cos(\phi_x + 1) = 0 \tag{4.3}$$

with a non-convex Hamiltonian. The initial condition is set to be $\phi(x, 0) = -\cos(\pi x)$, with a 2-periodic boundary condition. We compute the result up to $t = 0.5/\pi^2$.

The L_1 and L_∞ errors and numerical orders of accuracy are reported in Table 3 for C-HWENO5-LW3 and C-HWENO5-NCERK4 schemes. Both schemes achieve their

Table 1 The linear advection equation $\phi_t + \phi_x = 0$, with $\phi(x, 0) = \sin(\pi x)$, and a periodic boundary condition. C-HWENO5-LW3 and C-HWENO5-NCERK4. $t = 2$. L_1 and L_∞ errors and orders of accuracy

N	C-HWENO5-LW3				C-HWENO5-NCERK4			
	L_1 error	Order	L_∞ error	Order	L_1 error	Order	L_∞ error	Order
10	6.78E-02		9.49E-02		6.94E-02		9.68E-02	
20	3.11E-03	4.45	4.92E-03	4.27	3.16E-03	4.46	4.96E-03	4.29
40	9.47E-05	5.04	1.78E-04	4.79	9.69E-05	5.03	1.81E-04	4.78
80	3.03E-06	4.96	5.83E-06	4.94	3.06E-06	4.98	5.88E-06	4.94
160	9.74E-08	4.96	1.84E-07	4.99	9.64E-08	4.99	1.82E-07	5.01
320	3.16E-09	4.95	5.89E-09	4.96	3.01E-09	5.00	5.65E-09	5.01
640	1.13E-10	4.80	1.95E-10	4.92	9.38E-11	5.00	1.64E-10	5.10

Table 2 Burgers equation $\phi_t + (\phi_x + 1)^2/2 = 0$, with $\phi(x, 0) = -\cos(\pi x)$, and a periodic boundary condition. C-HWENO5-LW3 and C-HWENO5-NCERK4. $t = 0.5/\pi^2$. L_1 and L_∞ errors and orders of accuracy

N	C-HWENO5-LW3				C-HWENO5-NCERK4			
	L_1 error	Order	L_∞ error	Order	L_1 error	Order	L_∞ error	Order
10	1.35e-02		2.37e-02		1.35e-02		2.37e-02	
20	6.70e-04	4.33	2.31e-03	3.36	6.72e-04	4.33	2.32e-03	3.36
40	3.04e-05	4.46	1.70e-04	3.76	3.05e-05	4.46	1.71e-04	3.76
80	1.18e-06	4.69	1.03e-05	4.04	1.18e-06	4.69	1.03e-05	4.05
160	3.88e-08	4.93	4.17e-07	4.63	3.85e-08	4.94	4.17e-07	4.63
320	1.22e-09	4.99	1.41e-08	4.89	1.23e-09	4.97	1.42e-08	4.88
640	3.71e-11	5.04	3.89e-10	5.18	3.77e-11	5.03	3.91e-10	5.18

designed fifth-order accuracy with comparable errors. For this example and example 4.5, there are some fluctuations in numerical orders (especially for the L_∞ order) when the mesh is not very fine. The accuracy approaches the fifth-order eventually.

Example 4.4 We consider the nonlinear scalar Burgers equation in two dimensions

$$\phi_t + \frac{(\phi_x + \phi_y + 1)^2}{2} = 0 \tag{4.4}$$

with the initial condition $\phi(x, y, 0) = -\cos(\pi(x + y)/2)$, and a 4-periodic boundary condition in each direction. When $t = 0.5/\pi^2$ the solution is still smooth.

The L_1 and L_∞ errors and numerical orders of accuracy are presented in Table 4 for C-HWENO5-LW3 and C-HWENO5-NCERK4 schemes. Both schemes achieve their designed fifth-order accuracy with comparable errors.

Table 3 One-dimensional nonlinear problem with the non-convex Hamiltonian $H(\phi_x) = -\cos(\phi_x + 1)$, with $\phi(x, 0) = -\cos(\pi x)$, and a periodic boundary condition. C-HWENO5-LW3 and C-HWENO5-NCERK4. $t = 0.5/\pi^2$. L_1 and L_∞ errors and orders of accuracy

N	C-HWENO5-LW3				C-HWENO5-NCERK4			
	L_1 error	Order	L_∞ error	Order	L_1 error	Order	L_∞ error	Order
10	2.92E-03		7.24E-03		2.92E-03		7.30E-03	
20	3.05E-04	3.26	9.26E-04	2.97	3.10E-04	3.23	9.44E-04	2.95
40	2.09E-05	3.87	1.26E-04	2.88	2.10E-05	3.88	1.30E-04	2.86
80	1.46E-06	3.84	1.37E-05	3.20	1.45E-06	3.86	1.37E-05	3.25
160	7.67E-08	4.25	2.00E-06	2.77	7.61E-08	4.25	2.03E-06	2.75
320	2.61E-09	4.88	8.92E-08	4.49	2.61E-09	4.87	8.94E-08	4.50
640	5.52E-11	5.56	1.19E-09	6.23	5.52E-11	5.56	1.19E-09	6.23

Table 4 Burgers equation $\phi_t + (\phi_x + \phi_y + 1)^2/2 = 0$, with $\phi(x, y, 0) = -\cos(\pi(x + y)/2)$, and periodic boundary conditions. C-HWENO5-LW3 and C-HWENO5-NCERK4. $t = 0.5/\pi^2$. L_1 and L_∞ errors and orders of accuracy

$N_x \times N_y$	C-HWENO5-LW3				C-HWENO5-NCERK4			
	L_1 error	Order	L_∞ error	Order	L_1 error	Order	L_∞ error	Order
10×10	2.21e-02		5.44e-02		2.21e-02		5.45e-02	
20×20	1.26e-03	4.13	3.71e-03	3.87	1.27e-03	4.13	3.72e-03	3.87
40×40	6.11e-05	4.37	2.98e-04	3.64	6.13e-05	4.37	2.98e-04	3.64
80×80	2.37e-06	4.69	1.79e-05	4.06	2.37e-06	4.69	1.79e-05	4.06
160×160	7.74e-08	4.94	7.95e-07	4.49	7.71e-08	4.94	7.97e-07	4.49
320×320	2.42e-09	5.00	2.65e-08	4.91	2.42e-09	4.99	2.65e-08	4.91
640×640	7.09e-11	5.09	6.80e-10	5.28	7.15e-11	5.08	6.81e-10	5.28

Example 4.5 We here consider the following nonlinear scalar two-dimensional Hamilton-Jacobi equation

$$\phi_t - \cos(\phi_x + \phi_y + 1) = 0 \tag{4.5}$$

with a non-convex Hamiltonian. The initial condition is set to be $\phi(x, y, 0) = -\cos(\pi(x + y)/2)$, with a 4-periodic boundary condition in each direction. We compute the result until $t = 0.5/\pi^2$.

The L_1 and L_∞ errors and numerical orders of accuracy are reported in Table 5 for C-HWENO5-LW3 and C-HWENO5-NCERK4 schemes. Both schemes achieve their designed fifth-order accuracy with comparable errors.

Table 5 Two-dimensional nonlinear problem with the non-convex Hamiltonian $H(\phi_x, \phi_y) = -\cos(\phi_x + \phi_y + 1)$, with $\phi(x, y, 0) = -\cos(\pi(x + y)/2)$, and periodic boundary conditions. C-HWENO5-LW3 and C-HWENO5-NCERK4. $t = 0.5/\pi^2$. L_1 and L_∞ errors and orders of accuracy

$N_x \times N_y$	C-HWENO5-LW3				C-HWENO5-NCERK4			
	L_1 error	Order	L_∞ error	Order	L_1 error	Order	L_∞ error	Order
10×10	6.76e-03		1.36e-02		6.78e-03		1.37e-02	
20×20	4.37e-04	3.95	1.52e-03	3.16	4.42e-04	3.94	1.55e-03	3.14
40×40	3.69e-05	3.57	2.11e-04	2.85	3.70e-05	3.58	2.15e-04	2.85
80×80	2.43e-06	3.92	1.99e-05	3.41	2.42e-06	3.93	2.04e-05	3.40
160×160	1.44e-07	4.08	2.68e-06	2.89	1.44e-07	4.08	2.71e-06	2.91
320×320	4.30e-09	5.07	1.11e-07	4.59	4.29e-09	5.06	1.11e-07	4.61
640×640	9.41e-11	5.51	2.32e-09	5.58	9.42e-11	5.51	2.33e-09	5.58

4.2 Test cases with discontinuous derivatives

We now test the performance of the proposed methods in terms of their resolution and non-oscillatory property when solving problems with discontinuous derivatives.

Example 4.6 We consider the same one-dimensional linear equation (4.1) and the periodic boundary condition as in Example 4.1 but with non-smooth initial data $\phi(x, 0) = \phi_0(x - 0.5)$, where

$$\phi_0(x) = -\left(\frac{\sqrt{3}}{2} + \frac{9}{2} + \frac{2\pi}{3}\right)(x+1) + \begin{cases} 2 \cos\left(\frac{3\pi x^2}{2}\right) - \sqrt{3}, & -1 \leq x < -\frac{1}{3}, \\ \frac{3}{2} + 3 \cos(2\pi x), & -\frac{1}{3} \leq x < 0, \\ \frac{15}{2} - 3 \cos(2\pi x), & 0 \leq x < \frac{1}{3}, \\ \frac{28+4\pi+\cos(3\pi x)}{3} + 6\pi x(x-1), & \frac{1}{3} \leq x < 1. \end{cases} \quad (4.6)$$

We present the numerical solutions at $t = 2$ and $t = 8$ with $N = 100$ mesh elements. In Fig. 1, the solutions of C-HWENO5-LW3 and C-HWENO5-NCERK4 schemes are plotted, together with the exact solutions. We can see that both schemes lead to results with good resolution.

Example 4.7 We consider the same one-dimensional Burgers equation (4.2) as in Example 4.2 with the same initial and boundary conditions, except that we now present the numerical solutions at $t = 3.5/\pi^2$ when discontinuous derivative has already appeared in the solution. The Hamiltonian is nonlinear and convex. In Fig. 2, the solutions of C-HWENO5-LW3 and C-HWENO5-NCERK4 schemes are plotted, together with the exact solution. The mesh is uniform with $N = 80$ elements. We can see that both schemes give good results for this problem.

Example 4.8 We consider the same one-dimensional nonlinear equation (4.3) as in Example 4.3 with the same initial and boundary conditions, except that we now

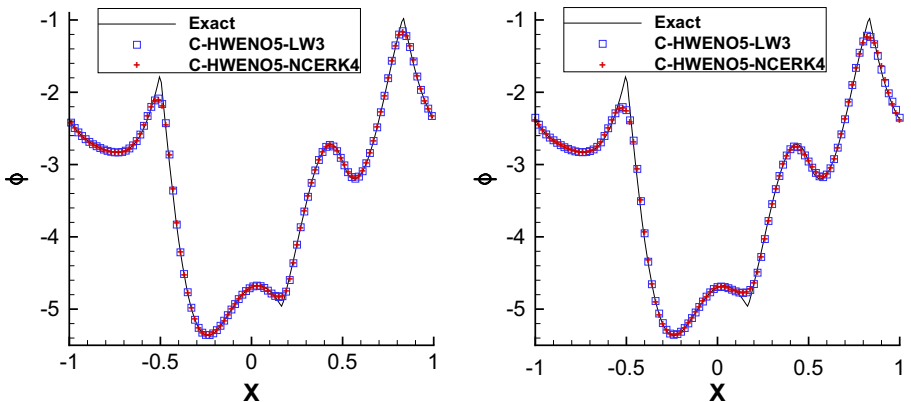


Fig. 1 Linear equation in one dimension. $t = 2$ (left) and $t = 8$ (right) with $N = 100$. Solid line: exact solution; square: C-HWENO5-LW3; plus: C-HWENO5-NCERK4

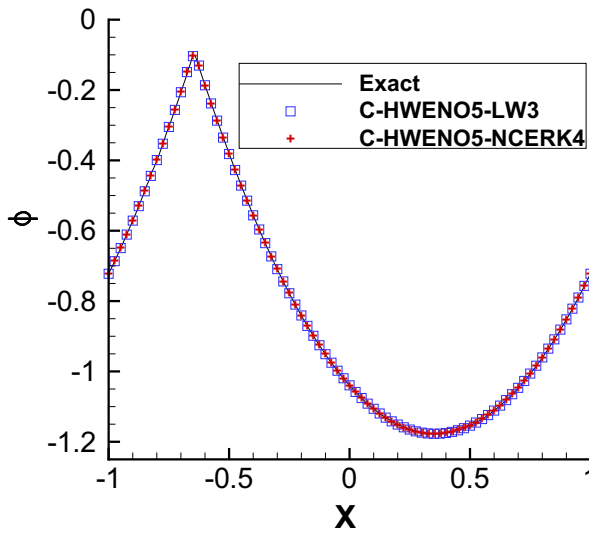


Fig. 2 Burgers equation in one dimension. $\phi(x, 0) = -\cos(\pi x)$. $t = 3.5/\pi^2$ and $N = 80$. Solid line: exact solution; square: C-HWENO5-LW3; plus: C-HWENO5-NCERK4

present the numerical solutions at $t = 1.5/\pi^2$ when discontinuous derivative has already appeared in the solution. The problem involves a non-convex Hamiltonian. In Fig. 3, the solutions of C-HWENO5-LW3 and C-HWENO5-NCERK4 schemes

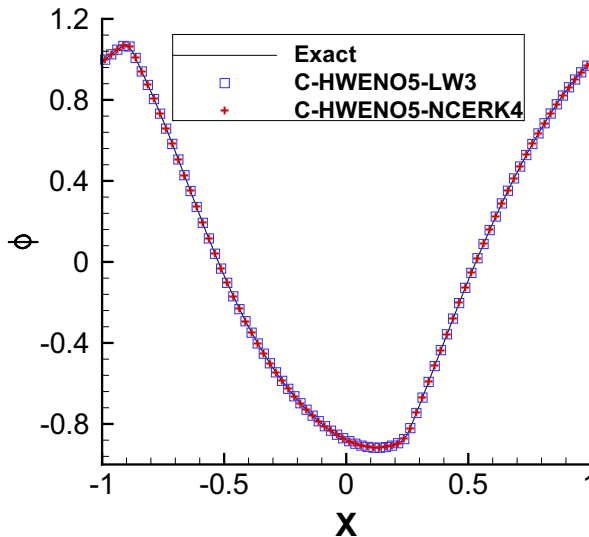


Fig. 3 Problem with the non-convex Hamiltonian $H(\phi_x) = -\cos(\phi_x + 1)$. $t = 1.5/\pi^2$ and $N = 80$. Solid line: exact solution; square: C-HWENO5-LW3; plus: C-HWENO5-NCERK4

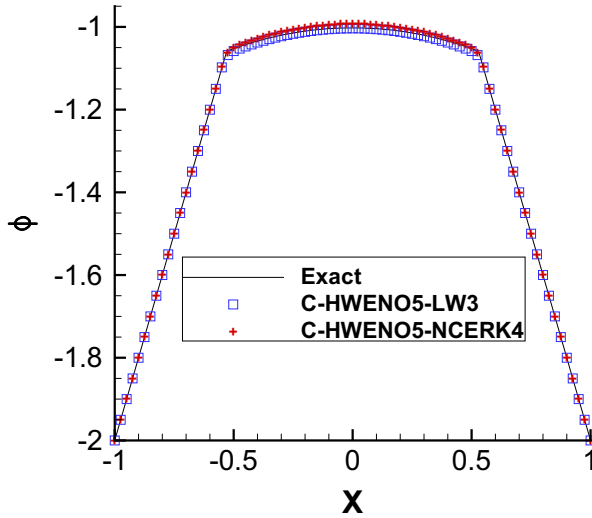


Fig. 4 Riemann problem with the non-convex Hamiltonian $H(\phi_x) = \frac{1}{4}(\phi_x^2 - 1)(\phi_x^2 - 4)$. $t = 1$ and $N = 80$. Solid line: exact solution; square: C-HWENO5-LW3; plus: C-HWENO5-NCERK4

are shown with $N = 80$ mesh elements, together with the exact solution. We can see that both schemes capture non-smooth features in the solution with good resolution.

Example 4.9 We consider the one-dimensional Riemann problem with a non-convex Hamiltonian

$$\begin{cases} \phi_t + \frac{1}{4}(\phi_x^2 - 1)(\phi_x^2 - 4) = 0, & -1 < x < 1, \\ \phi(x, 0) = -2|x|. \end{cases} \quad (4.7)$$

This is a demanding test case, for many schemes have poor resolutions or could even converge to a non-viscosity solution for this case. In Fig. 4, we plot the solutions at $t = 1$ by C-HWENO5-LW3 and C-HWENO5-NCERK4 schemes with $N = 80$ mesh elements, together with the exact solution. We can observe that both schemes show good resolution for this problem.

Example 4.10 We solve the same two-dimensional Burgers equation (4.4) as in Example 4.4 with the same initial and boundary conditions, except that we now present the numerical solutions at $t = 1.5/\pi^2$ when the discontinuous derivative has already appeared in the solution. In Fig. 5, we show the contours and surfaces of the computed solutions on a 40×40 mesh by C-HWENO5-LW3 and C-HWENO5-NCERK4 schemes. Both schemes have good resolution for this problem.

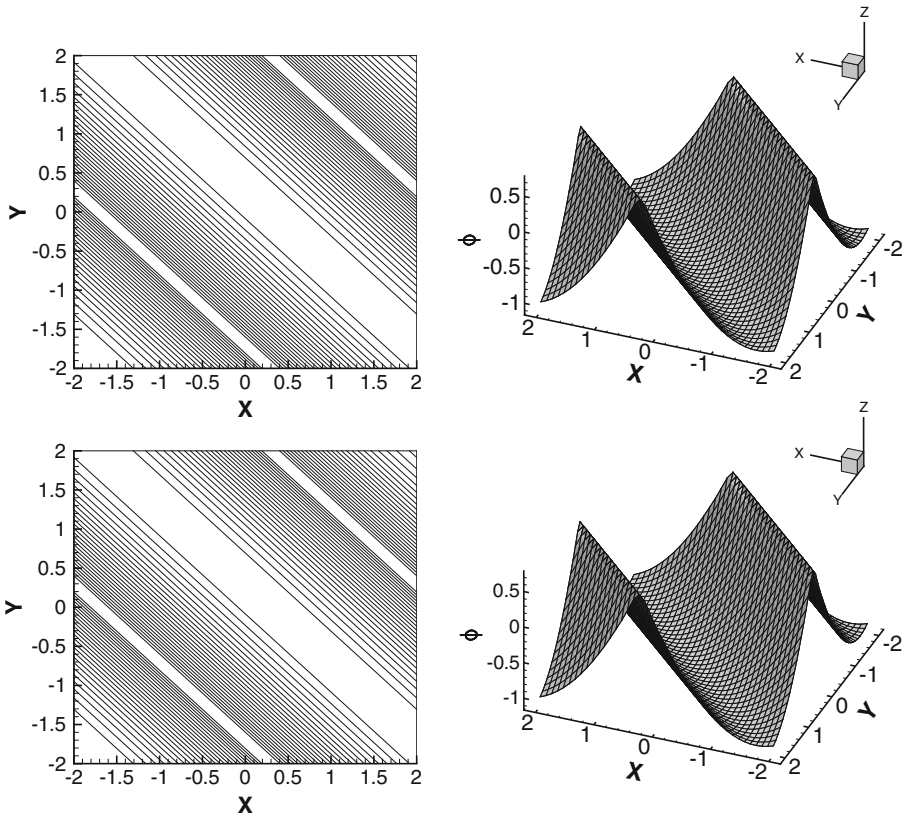


Fig. 5 Burgers equation in two dimensions. $t = 1.5/\pi^2$ and $N_x \times N_y = 40 \times 40$. The contour (left) and surface (right) of solutions computed by C-HWENO5-LW3 (top) and C-HWENO5-NCERK4 (bottom)

Example 4.11 The two-dimensional Riemann problem with a non-convex Hamiltonian

$$\begin{cases} \phi_t + \sin(\phi_x + \phi_y) = 0, & -1 \leq x, y < 1, \\ \phi(x, y, 0) = \pi(|y| - |x|). \end{cases} \quad (4.8)$$

We compute up to $t = 1$. In Fig. 6, the contours and surfaces of the computed solutions are presented on an 80×80 mesh by C-HWENO5-LW3 and C-HWENO5-NCERK4 schemes. We observe good resolution for both schemes.

Example 4.12 A problem from optimal control

$$\begin{cases} \phi_t + \sin(y)\phi_x + (\sin(x) + \text{sign}(\phi_y))\phi_y - \frac{1}{2}\sin(y)^2 - (1 - \cos(x)) = 0, & -\pi \leq x, y < \pi, \\ \phi(x, y, 0) = 0. \end{cases} \quad (4.9)$$

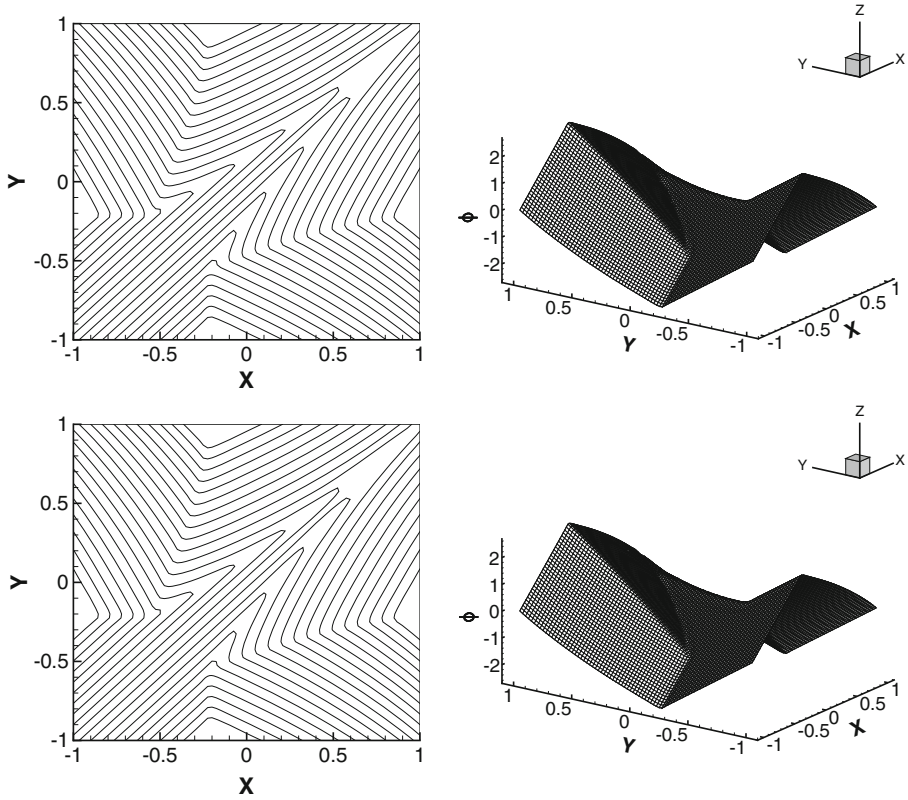


Fig. 6 Two-dimensional Riemann problem with a non-convex Hamiltonian $H(\phi_x, \phi_y) = \sin(\phi_x + \phi_y)$. $t = 1$ and $N_x \times N_y = 80 \times 80$. The contour (left) and surface (right) of solutions computed by C-HWENO5-LW3 (top) and C-HWENO5-NCERK4 (bottom)

with the periodic boundary condition, see [27]. We compute up to $t = 1$. In Fig. 7, the surfaces of the solutions and the optimal control $\omega = \sin(\phi_y)$ are reported on a 60×60 mesh by C-HWENO5-LW3 and C-HWENO5-NCERK4 schemes. Good resolution is observed with both schemes.

Example 4.13 A two-dimensional Eikonal equation with a non-convex Hamiltonian, which arises in geometric optics [15], is given by

$$\begin{cases} \phi_t + \sqrt{\phi_x^2 + \phi_y^2} + 1 = 0, & 0 \leq x, y < 1, \\ \phi(x, y, 0) = \frac{1}{4}(\cos(2\pi x) - 1)(\cos(2\pi y) - 1) - 1. \end{cases} \quad (4.10)$$

with the periodic boundary condition. We compute up to $t = 0.6$. In Fig. 8, We present the contours and surfaces of the computed solutions on an 80×80 mesh by

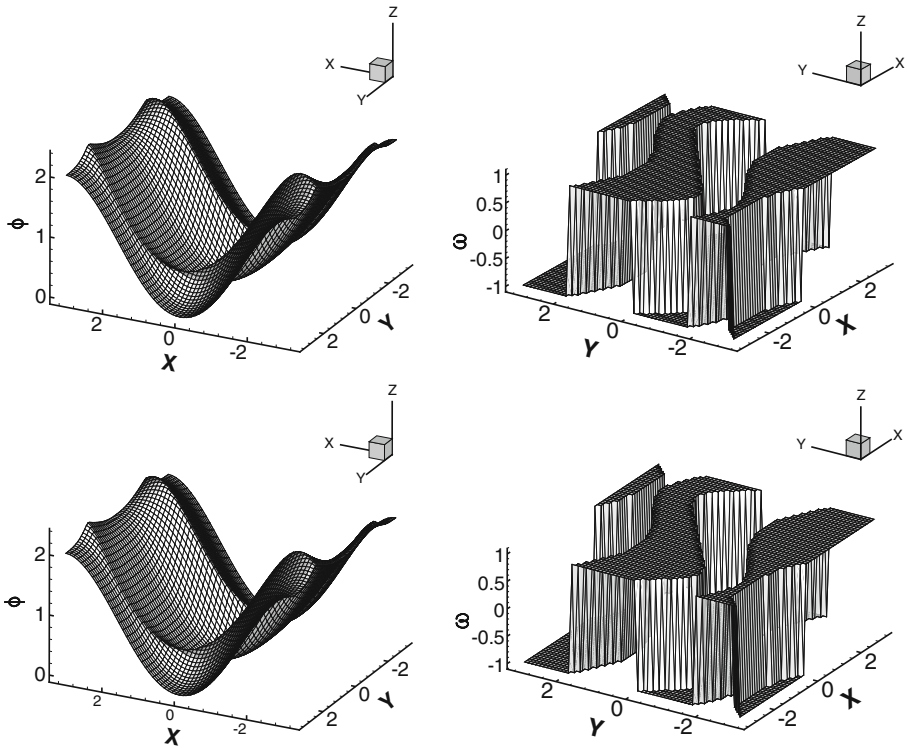


Fig. 7 The optimal control problem. $t = 1$ and $N_x \times N_y = 60 \times 60$. The surface of solutions (left) and the optimal control $\omega = \sin(\phi_y)$ (right) computed by C-HWENO5-LW3 (top) and C-HWENO5-NCERK4 (bottom)

C-HWENO5-LW3 and C-HWENO5-NCERK4 schemes. Both schemes show good resolution to approximate the solution with comparable results.

Example 4.14 A problem of a propagating surface [26] is governed by

$$\begin{cases} \phi_t - (1 - \varepsilon K)\sqrt{\phi_x^2 + \phi_y^2 + 1} = 0, & 0 \leq x, y < 1, \\ \phi(x, y, 0) = 1 - \frac{1}{4}(\cos(2\pi x) - 1)(\cos(2\pi y) - 1). \end{cases} \quad (4.11)$$

where K is the mean curvature defined by

$$K = -\frac{\phi_{xx}(1 + \phi_y^2) - 2\phi_{xy}\phi_x\phi_y + \phi_{yy}(1 + \phi_x^2)}{(1 + \phi_x^2 + \phi_y^2)^{\frac{3}{2}}},$$

and ε is a small constant. A periodic boundary condition is used.

In Fig. 9, We present the results of $\varepsilon = 0$ (pure convection) and $\varepsilon = 0.1$ on a 60×60 mesh by C-HWENO5-LW3 and C-HWENO5-NCERK4 schemes. The

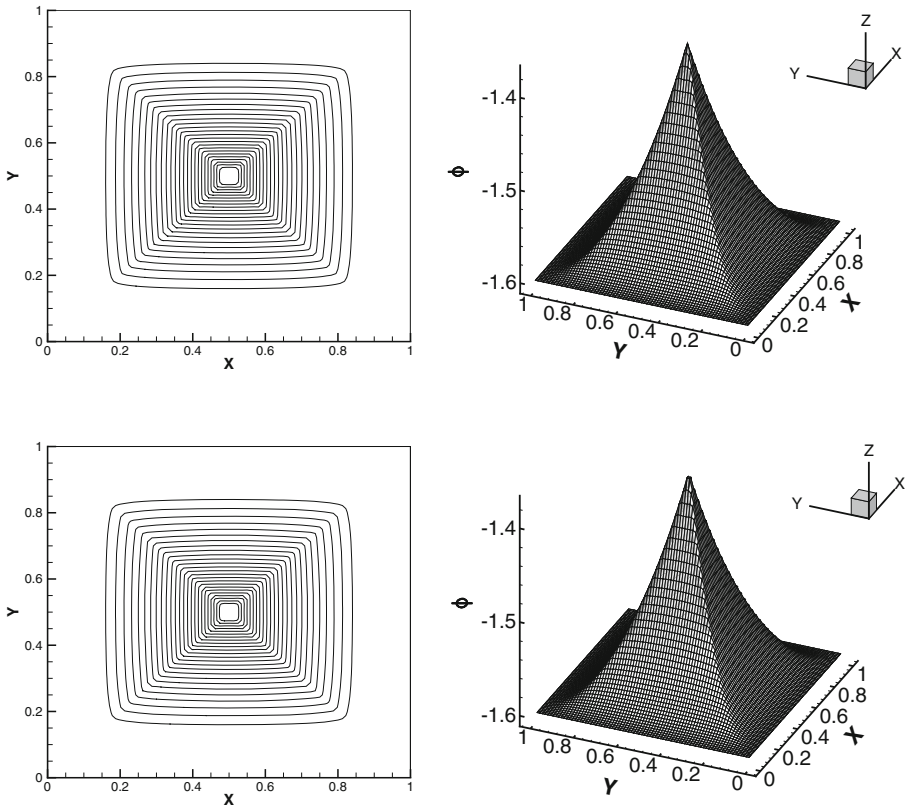


Fig. 8 Eikonal equation (4.10) with a non-convex Hamiltonian $H(\phi_x, \phi_y) = \sqrt{\phi_x^2 + \phi_y^2} + 1$, $t = 0.6$ and $N_x \times N_y = 80 \times 80$. The contour (left) and surface (right) of solutions computed by C-HWENO5-LW3 (top) and C-HWENO5-NCERK4 (bottom)

surfaces at $t = 0$ for $\varepsilon = 0$ and for $\varepsilon = 0.1$, and at $t = 0.1$ for $\varepsilon = 0.1$, are shifted downward in order to show the detail of the solution at later time. Both schemes show good resolution to approximate the solution with comparable results.

Example 4.15 We solve the two-dimensional Eikonal equation

$$\phi_t + \sqrt{\phi_x^2 + \phi_y^2} = 1. \tag{4.12}$$

- (1) We consider the case of the computational domain being $[0, 1]^2 \setminus [0.4, 0.6]^2$. For the inner boundary cells inside $[0.4, 0.6]^2$, we impose the exact solution that is minus distance function to the inner boundary. On the other hand, we impose free outflow boundary conditions on the outer boundary. The initial

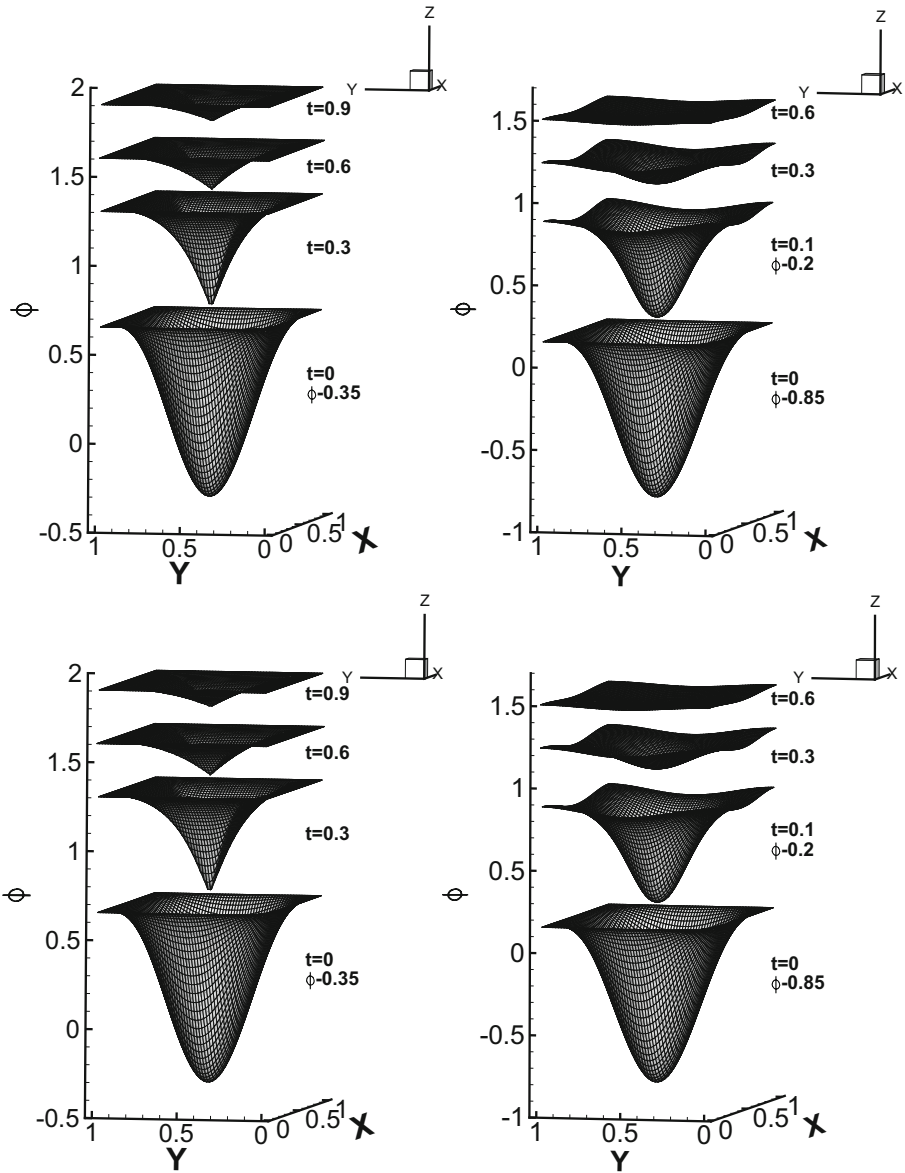


Fig. 9 Propagating surface. $N_x \times N_y = 60 \times 60$. $\varepsilon = 0$ (left) and $\varepsilon = 0.1$ (right) computed by C-HWENO5-LW3 (top) and C-HWENO5-NCERK4 (bottom)

condition is taken as $\phi_0(x, y) = \max\{|x-0.5|, |y-0.5|\} - 0.1$. The steady state solution should give us a function that is equal to distance of the point to the inner boundary. In Fig. 10, we plot the contours and surfaces of the numerical

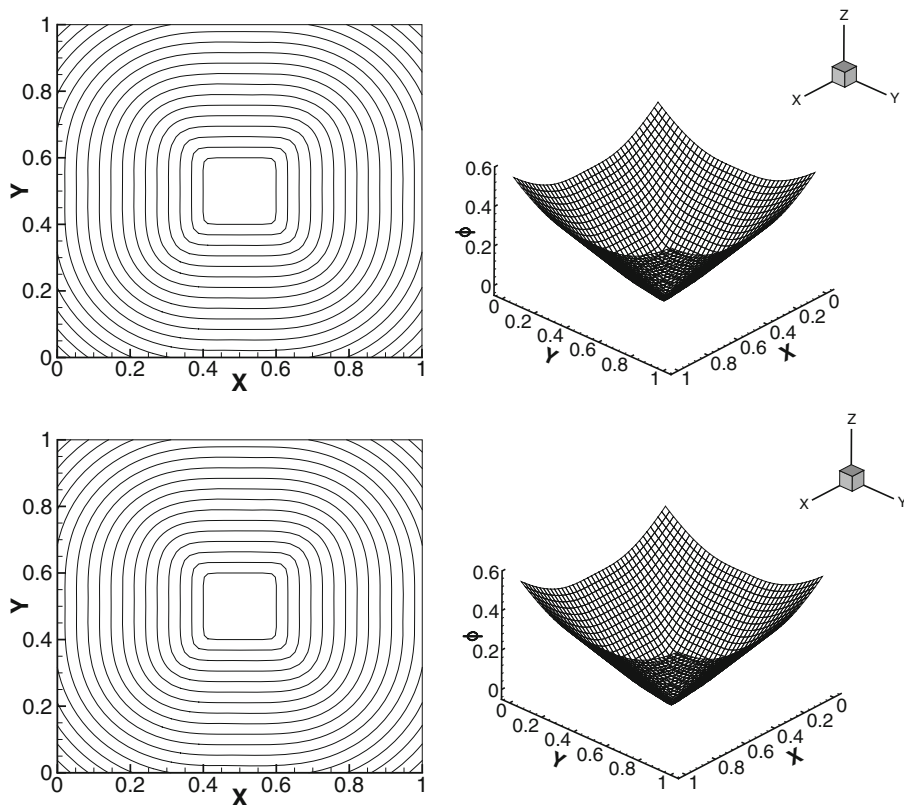


Fig. 10 Steady state solution of the two-dimensional Eikonal equation (4.12): case (1). $N_x \times N_y = 40 \times 40$. The contour (left) and surface (right) of solutions computed by C-HWENO5-LW3 (top) and C-HWENO5-NCERK4 (bottom)

steady state solution with 40×40 mesh elements by C-HWENO5-LW3 and C-HWENO5-NCERK4 schemes.

- (2) We consider this example with a point source condition. Namely, we take the inner boundary to be the center point $(0.5, 0.5)$. In this case, we use the exact distance function to the center point for ϕ in the center cells. For the primal mesh, we have one center cell and $(0.5, 0.5)$ is the center point of this cell. For the dual mesh, we have four center cells and $(0.5, 0.5)$ is one of the corner grid points of these four cells. The outer boundary conditions are the same as for the previous case. The initial condition is taken as $\phi_0(x, y) = \max\{|x - 0.5|, |y - 0.5|\}$. In Fig. 11, we plot the contours and surfaces of the numerical steady state solution with 39×39 mesh elements by C-HWENO5-LW3 and C-HWENO5-NCERK4 schemes. We can see that both schemes obtain very good resolution to the viscosity solution in both cases.

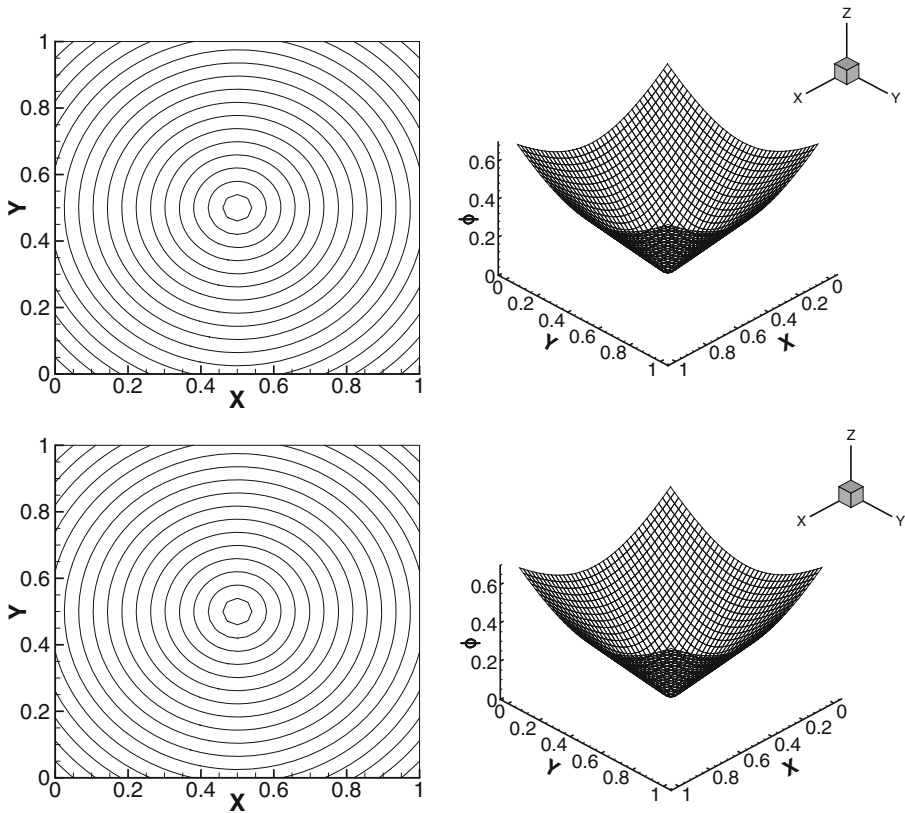


Fig. 11 Steady state solution of the two-dimensional Eikonal equation (4.12): case (2). $N_x \times N_y = 39 \times 39$. The contour (left) and surface (right) of solutions computed by C-HWENO5-LW3 (top) and C-HWENO5-NCERK4 (bottom)

5 Concluding remarks

In this paper, we design a new class of high-order central Hermite WENO schemes for directly solving HJ equations in one- and two-dimension. The methods use Hermite WENO reconstruction based on moments of the solution as spatial discretizations, and Lax-Wendroff type methods or the natural continuous extension of Runge-Kutta methods as time discretizations, in a central finite volume framework on staggered meshes. Our schemes evolve in time the moments of the solution rather than the solution and its derivative(s) for the spatial reconstruction, meanwhile having the advantage of being compact. Due to the inclusion of the mixed first-order moment \overline{vw}_{ij}^n , one major advantage of our schemes is that the two-dimensional HWENO spatial reconstruction can be implemented through a dimension-by-dimension strategy. In other words, the proposed HWENO spatial reconstructions in one dimension are

employed directly in two or higher dimensions, and lead to an easier multidimensional simulations. In addition, a key ingredient for directly solving HJ equations is the reconstruction of numerical Hamiltonians to guarantee the stability of methods. Benefited from the central strategy, our methods require no numerical Hamiltonians which makes the schemes simpler. Our schemes combine the HWENO spatial reconstructions and the central scheme and therefore carry many features of both schemes. Instead of working with staggered meshes, the proposed spatial reconstructions can also be applied to the central finite volume schemes defined on two overlapping meshes [24].

Acknowledgments The research was partially supported by NSFC grant 11571290 and NSAF grant U1630247.

Appendix A

When we apply the central Hermite WENO scheme with Lax-Wendroff time discretization in Section 2.2 to solve the two-dimensional example 4.14 in Section 4, one can see that the Hamiltonian H of this example depends on not only the first derivatives ϕ_x, ϕ_y , but also three second derivatives $\phi_{xx}, \phi_{xy}, \phi_{yy}$. If we still convert time derivatives into spatial ones as in Eq. 2.30, this can become very involved. Alternatively, following the idea in [28, 29], we use the following Lax-Wendroff procedure which produces the best balance between cost reduction and ensuring ENO properties for the reconstruction.

Recall that based on Eqs. 2.25-2.29, one will need to reconstruct at the current time $t^n, \forall i, j$,

- (1) the moments $\bar{\phi}_{i+1/2,j+1/2}^n, \bar{v}_{i+1/2,j+1/2}^n, \bar{w}_{i+1/2,j+1/2}^n$ and $\bar{vw}_{i+1/2,j+1/2}^n$ on the dual mesh, as well as
- (2) the point value of $F(x_*, y_*, t^n)$ with $(x_*, y_*) \in \mathcal{G}$. Note that $F = \Delta t H + \frac{\Delta t^2}{2} \frac{\partial}{\partial t} H + \frac{\Delta t^3}{6} \frac{\partial^2}{\partial t^2} H$.

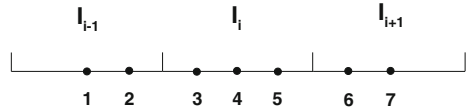
The staggered moments $\bar{\phi}_{i+1/2,j+1/2}^n, \bar{v}_{i+1/2,j+1/2}^n, \bar{w}_{i+1/2,j+1/2}^n$ and $\bar{vw}_{i+1/2,j+1/2}^n$ on the dual mesh are reconstructed by the same procedure as in Section 2.2. The remainder is to approximate the point value of $F(x_*, y_*, t^n)$. More specifically, we need to approximate the point values of $H, \frac{\partial}{\partial t} H$ and $\frac{\partial^2}{\partial t^2} H$ at (x_*, y_*, t^n) . Since the data before and after the reconstruction is all at the same time level t^n , the superscript n will be omitted below, together with the dependence on the time t .

Step 1: A reconstruction for $H(\phi_x, \phi_y, \phi_{xx}, \phi_{xy}, \phi_{yy})$ at (x_*, y_*) .

The reconstruction of point values of $q(x_*, y_*)$, where $q = \phi_x, \phi_y, \phi_{xx}, \phi_{xy}$, or ϕ_{yy} are the same as in Section 2.2. Then we can get the approximation of $H(\phi_x, \phi_y, \phi_{xx}, \phi_{xy}, \phi_{yy})$ as well as ϕ_t at (x_*, y_*)

$$\phi_t|_{(x_*, y_*)} = -H(\phi_x, \phi_y, \phi_{xx}, \phi_{xy}, \phi_{yy})|_{(x_*, y_*)}.$$

Fig. 12 One-dimensional Gauss-Lobatto points in the cells $\{I_{i-1/2}, I_{i+1/2}\}$



Step 2: A reconstruction for the first temporal derivative of $H(\phi_x, \phi_y, \phi_{xx}, \phi_{xy}, \phi_{yy})$ at (x_*, y_*) .

According to the Hamiltonian H in example 4.14, we have

$$\frac{\partial}{\partial t} H(\phi_x, \phi_y, \phi_{xx}, \phi_{xy}, \phi_{yy}) = H_1 \phi_{xt} + H_2 \phi_{yt} + H_3 \phi_{xxt} + H_4 \phi_{xyt} + H_5 \phi_{yyt},$$

where H_1 and H_2 are functions depend on $\phi_x, \phi_y, \phi_{xx}, \phi_{xy}$ and ϕ_{yy} , while H_3, H_4 and H_5 are functions depend on ϕ_x and ϕ_y . In order to reconstruct $\frac{\partial}{\partial t} H$, we only need to reconstruct $\phi_{xt}, \phi_{yt}, \phi_{xxt}, \phi_{xyt}$ and ϕ_{yyt} which are given as below.

We first consider one-dimensional case. Suppose we have primal mesh $\{I_i\}_i$ and dual mesh $\{I_{i+1/2}\}_i$. For any given i , consider all the Gauss-Lobatto quadrature points in the cells $I_{i-1/2}$ and $I_{i+1/2}$, relabeled as p_1, \dots, p_7 , namely

$$\begin{aligned} p_1 &= x_{i-1}, & p_2 &= x_{i-\frac{1}{2}-\frac{\sqrt{5}}{10}}, & p_3 &= x_{i-\frac{1}{2}+\frac{\sqrt{5}}{10}}, & p_4 &= x_i, \\ p_4 &= x_i, & p_5 &= x_{i+\frac{1}{2}-\frac{\sqrt{5}}{10}}, & p_6 &= x_{i+\frac{1}{2}+\frac{\sqrt{5}}{10}}, & p_7 &= x_{i+1}. \end{aligned}$$

Note that the points p_1, \dots, p_7 are interior points with respect to the primal mesh, see Fig. 12.

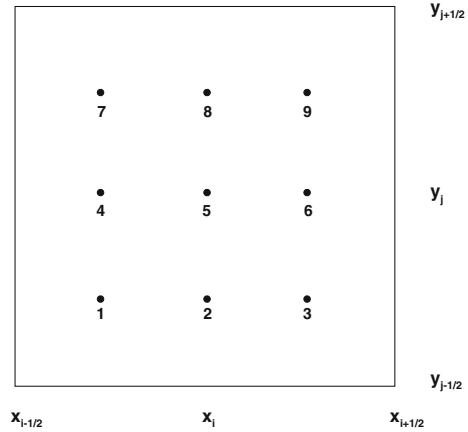
Let g_n denote the point value of a function g at point p_n , namely, $g_n = g(p_n), n = 1, \dots, 7$. We introduce a simple one-dimensional fourth-order ‘‘central’’ difference formula to approximate the first derivative $g_x(p_n)$ with $n = 3, 4, 5$ in the target cell I_i

$$\begin{aligned} g_x(p_3) &= \frac{1}{\Delta x} \left[\frac{(4\sqrt{5}-6)}{11} g_1 - (\sqrt{5}-1) g_2 - \frac{(5+\sqrt{5})}{4} g_3 \right. \\ &\quad \left. + (\sqrt{5}+1) g_4 - \frac{(5\sqrt{5}+9)}{44} g_5 \right], \\ g_x(p_4) &= \frac{1}{2\Delta x} \left[(\sqrt{5}-2) g_2 - (\sqrt{5}+2) g_3 + (\sqrt{5}+2) g_5 - (\sqrt{5}-2) g_6 \right], \quad (\text{A.1}) \\ g_x(p_5) &= \frac{1}{\Delta x} \left[\frac{(5\sqrt{5}+9)}{44} g_3 - (\sqrt{5}+1) g_4 + \frac{(5+\sqrt{5})}{4} g_5 \right. \\ &\quad \left. + (\sqrt{5}-1) g_6 - \frac{(4\sqrt{5}-6)}{11} g_7 \right], \end{aligned}$$

as well as a one-dimensional third-order ‘‘central’’ difference formula to approximate the second derivative $g_{xx}(p_n)$ with $n = 3, 4, 5$ in the target cell I_i

$$\begin{aligned} g_{xx}(p_3) &= \frac{1}{\Delta x^2} \left[(5-3\sqrt{5}) g_1 + 10 g_2 - 20 g_3 + (5+3\sqrt{5}) g_4 \right], \\ g_{xx}(p_4) &= \frac{1}{2\Delta x^2} \left[(15-7\sqrt{5}) g_2 + (15+7\sqrt{5}) g_3 \right. \\ &\quad \left. - 60 g_4 + (15+7\sqrt{5}) g_5 + (15-7\sqrt{5}) g_6 \right], \quad (\text{A.2}) \\ g_{xx}(p_5) &= \frac{1}{\Delta x^2} \left[(5+3\sqrt{5}) g_4 - 20 g_5 + 10 g_6 + (5-3\sqrt{5}) g_7 \right]. \end{aligned}$$

Fig. 13 Two-dimensional Gauss-Lobatto quadrature nodes in \mathcal{G} located within I_{ij}



Back to our two-dimensional situation. We will apply the above “central” difference formulation multiple times based on a dimension-by-dimension procedure and relabel the Gauss-Lobatto quadrature points in the cell I_{ij} as $p_{ij}^1, \dots, p_{ij}^9$ as shown in Fig. 13 to assist with the presentation,

$$\begin{aligned}
 p_{i,j}^1 &= (x_{i-\frac{1}{2}+\frac{\sqrt{5}}{10}}, y_{j-\frac{1}{2}+\frac{\sqrt{5}}{10}}), p_{i,j}^2 = (x_i, y_{j-\frac{1}{2}+\frac{\sqrt{5}}{10}}), p_{i,j}^3 = (x_{i+\frac{1}{2}-\frac{\sqrt{5}}{10}}, y_{j-\frac{1}{2}+\frac{\sqrt{5}}{10}}), \\
 p_{i,j}^4 &= (x_{i-\frac{1}{2}+\frac{\sqrt{5}}{10}}, y_j), p_{i,j}^5 = (x_i, y_j), p_{i,j}^6 = (x_{i+\frac{1}{2}-\frac{\sqrt{5}}{10}}, y_j), \\
 p_{i,j}^7 &= (x_{i-\frac{1}{2}+\frac{\sqrt{5}}{10}}, y_{j+\frac{1}{2}-\frac{\sqrt{5}}{10}}), p_{i,j}^8 = (x_i, y_{j+\frac{1}{2}-\frac{\sqrt{5}}{10}}), p_{i,j}^9 = (x_{i+\frac{1}{2}-\frac{\sqrt{5}}{10}}, y_{j+\frac{1}{2}-\frac{\sqrt{5}}{10}}).
 \end{aligned}$$

By applying the formulation (A.1) along x direction,

- we reconstruct $\{\phi_{xt}(p_{i,j}^1), \phi_{xt}(p_{i,j}^2), \phi_{xt}(p_{i,j}^3)\}_{ij}$ based on $\{\phi_t(p_{i-1,j}^2), \phi_t(p_{i-1,j}^3), \phi_t(p_{i,j}^1), \phi_t(p_{i,j}^2), \phi_t(p_{i,j}^3), \phi_t(p_{i+1,j}^1), \phi_t(p_{i+1,j}^2)\}_{ij}$;
- we reconstruct $\{\phi_{xt}(p_{i,j}^4), \phi_{xt}(p_{i,j}^5), \phi_{xt}(p_{i,j}^6)\}_{ij}$ based on $\{\phi_t(p_{i-1,j}^5), \phi_t(p_{i-1,j}^6), \phi_t(p_{i,j}^4), \phi_t(p_{i,j}^5), \phi_t(p_{i,j}^6), \phi_t(p_{i+1,j}^4), \phi_t(p_{i+1,j}^5)\}_{ij}$;
- and we reconstruct $\{\phi_{xt}(p_{i,j}^7), \phi_{xt}(p_{i,j}^8), \phi_{xt}(p_{i,j}^9)\}_{ij}$ based on $\{\phi_t(p_{i-1,j}^8), \phi_t(p_{i-1,j}^9), \phi_t(p_{i,j}^7), \phi_t(p_{i,j}^8), \phi_t(p_{i,j}^9), \phi_t(p_{i+1,j}^7), \phi_t(p_{i+1,j}^8)\}_{ij}$.

ϕ_{xxt} can be computed following the similar procedure by the formulation (A.2) based on ϕ_t .

By applying the formulation (A.1) along y direction,

- we reconstruct $\{\phi_{yt}(p_{i,j}^1), \phi_{yt}(p_{i,j}^4), \phi_{yt}(p_{i,j}^7)\}_{ij}$ based on $\{\phi_t(p_{i,j-1}^4), \phi_t(p_{i,j-1}^7), \phi_t(p_{i,j}^1), \phi_t(p_{i,j}^4), \phi_t(p_{i,j}^7), \phi_t(p_{i,j+1}^1), \phi_t(p_{i,j+1}^4)\}_{ij}$;

- we reconstruct $\{\phi_{yt}(p_{i,j}^2), \phi_{yt}(p_{i,j}^5), \phi_{yt}(p_{i,j}^8)\}_{ij}$ based on $\{\phi_t(p_{i,j-1}^5), \phi_t(p_{i,j-1}^8), \phi_t(p_{i,j}^2), \phi_t(p_{i,j}^5), \phi_t(p_{i,j}^8), \phi_t(p_{i,j+1}^2), \phi_t(p_{i,j+1}^5)\}_{ij}$;
- and we reconstruct $\{\phi_{yt}(p_{i,j}^3), \phi_{yt}(p_{i,j}^6), \phi_{yt}(p_{i,j}^9)\}_{ij}$ based on $\{\phi_t(p_{i,j-1}^6), \phi_t(p_{i,j-1}^9), \phi_t(p_{i,j}^3), \phi_t(p_{i,j}^6), \phi_t(p_{i,j}^9), \phi_t(p_{i,j+1}^3), \phi_t(p_{i,j+1}^6)\}_{ij}$.

ϕ_{yyt} can be computed following the similar procedure by the formulation (A.2) based on ϕ_t .

Next, based on $\phi_{xt}(x_*, y_*)$, $(x_*, y_*) \in \mathcal{G}$, we can also apply formulation (A.1) to approximate $\phi_{xyt}(x_*, y_*)$ along y direction similar as the reconstruction of ϕ_{yt} .

Finally, we can get the approximation for the first temporal derivative of H as well as ϕ_{tt} at (x_*, y_*)

$$\begin{aligned} \phi_{tt}|_{(x_*, y_*)} &= -\frac{\partial}{\partial t} H(\phi_x, \phi_y, \phi_{xx}, \phi_{xy}, \phi_{yy})|_{(x_*, y_*)} \\ &= -(H_1\phi_{xt} + H_2\phi_{yt} + H_3\phi_{xxt} + H_4\phi_{xyt} + H_5\phi_{yyt})|_{(x_*, y_*)}. \end{aligned}$$

Step 3: A reconstruction for the second temporal derivative of $H(\phi_x, \phi_y, \phi_{xx}, \phi_{xy}, \phi_{yy})$ at (x_*, y_*) .

We also have

$$\begin{aligned} \frac{\partial^2}{\partial t^2} H(\phi_x, \phi_y, \phi_{xx}, \phi_{xy}, \phi_{yy}) &= (H_1\phi_{xt} + H_2\phi_{yt} + H_3\phi_{xxt} + H_4\phi_{xyt} + H_5\phi_{yyt})_t \\ &= (H_{11}\phi_{xt} + H_{12}\phi_{yt} + H_{13}\phi_{xxt} + H_{14}\phi_{xyt} \\ &\quad + H_{15}\phi_{yyt})\phi_{xt} + H_1\phi_{xtt} \\ &\quad + (H_{21}\phi_{xt} + H_{22}\phi_{yt} + H_{23}\phi_{xxt} + H_{24}\phi_{xyt} \\ &\quad + H_{25}\phi_{yyt})\phi_{yt} + H_2\phi_{ytt} \\ &\quad + (H_{31}\phi_{xt} + H_{32}\phi_{yt})\phi_{xxt} + H_3\phi_{xxtt} \\ &\quad + (H_{41}\phi_{xt} + H_{42}\phi_{yt})\phi_{xyt} + H_4\phi_{xytt} \\ &\quad + (H_{51}\phi_{xt} + H_{52}\phi_{yt})\phi_{yyt} + H_5\phi_{yytt}, \end{aligned}$$

where $H_1, H_2, H_{11}, H_{12}, H_{21}$ and H_{22} are functions depend on $\phi_x, \phi_y, \phi_{xx}, \phi_{xy}$ and ϕ_{yy} , while $H_3, H_4, H_5, H_{13}, H_{14}, H_{15}, H_{23}, H_{24}, H_{25}, H_{31}, H_{32}, H_{41}, H_{42}, H_{51}$ and H_{52} are functions depend on ϕ_x and ϕ_y . In order to reconstruct $\frac{\partial^2}{\partial t^2} H$, we only need to reconstruct $\phi_{xtt}, \phi_{ytt}, \phi_{xxtt}, \phi_{xytt}$ and ϕ_{yytt} which can be obtained based on ϕ_{tt} following the same procedure as in step 2 given above.

References

1. Augoula, S., Abgrall, R.: High order numerical discretization for Hamilton-Jacobi equations on triangular meshes. *J. Sci. Comput.* **15**, 197–229 (2000)
2. Barth, T.J., Sethian, J.A.: Numerical schemes for the Hamilton-Jacobi and level set equations on triangulated domains. *J. Comput. Phys.* **145**, 1–40 (1998)
3. Bianco, F., Puppo, G., Russo, G.: High-order central schemes for hyperbolic systems of conservation laws. *SIAM J. Sci. Comput.* **21**, 294–322 (1999)

4. Bryson, S., Levy, D.: Central schemes for multi-dimensional Hamilton-Jacobi equations. *SIAM J. Sci. Comput.* **25**, 767–791 (2003)
5. Bryson, S., Levy, D.: High-order central WENO schemes for multidimensional Hamilton-Jacobi equations. *SIAM J. Numer. Anal.* **41**, 1339–1369 (2003)
6. Bryson, S., Levy, D.: High-order semi-discrete central-upwind schemes for multi-dimensional Hamilton-Jacobi equations. *J. Comput. Phys.* **189**, 63–87 (2003)
7. Cheng, Y.D., Shu, C.-W.: A discontinuous Galerkin finite element method for directly solving the Hamilton-Jacobi equations. *J. Comput. Phys.* **223**, 398–415 (2007)
8. Cheng, Y.D., Wang, Z.: A new discontinuous Galerkin finite element method for directly solving the Hamilton-Jacobi equations. *J. Comput. Phys.* **268**, 134–153 (2014)
9. Crandall, M.G., Evans, L.C., Lions, P.L.: Some properties of viscosity solutions of Hamilton-Jacobi equations. *Trans. Am. Math. Soc.* **282**, 487–502 (1984)
10. Crandall, M.G., Lions, P.L.: Viscosity solutions of Hamilton-Jacobi equations. *Trans. Am. Math. Soc.* **277**, 1–42 (1983)
11. Dumbser, M., Balsara, D.S., Toro, E.F., Munz, C.-D.: A unified framework for the construction of one-step finite volume and discontinuous Galerkin schemes on unstructured meshes. *J. Comput. Phys.* **227**, 8209–8253 (2008)
12. Harten, A., Engquist, B., Osher, S., Chakravathy, S.: Uniformly high order accurate essentially non-oscillatory schemes, III. *J. Comput. Phys.* **71**, 231–303 (1987)
13. Hu, C., Shu, C.-W.: A discontinuous Galerkin finite element method for Hamilton-Jacobi equations. *SIAM J. Sci. Comput.* **21**, 666–690 (1998)
14. Jiang, G., Peng, D.: Weighted ENO schemes for Hamilton-Jacobi equations. *SIAM J. Sci. Comput.* **21**, 2126–2143 (1999)
15. Jin, S., Xin, Z.: Numerical passage from systems of conservation laws to Hamilton-Jacobi equations, and relaxation schemes. *SIAM J. Numer. Anal.* **35**, 2385–2404 (1998)
16. Kurganov, A., Tadmor, E.: New high-resolution semi-discrete central schemes for Hamilton-Jacobi equations. *J. Comput. Phys.* **160**, 720–742 (2000)
17. Lafon, F., Osher, S.: High order two-dimensional nonoscillatory methods for solving Hamilton-Jacobi scalar equations. *J. Comput. Phys.* **123**, 235–253 (1996)
18. Lax, P.D., Wendroff, B.: Systems of conservation laws. *Commun. Pure Appl. Math.* **13**, 217–237 (1960)
19. Lepsky, O., Hu, C., Shu, C.-W.: Analysis of the discontinuous Galerkin method for Hamilton-Jacobi equations. *Appl. Numer. Math.* **33**, 423–434 (2000)
20. Li, F., Yakovlev, S.: A central discontinuous Galerkin method for Hamilton-Jacobi equations. *J. Sci. Comput.* **45**, 404–428 (2010)
21. Li, X.G., Chan, C.K.: High-order schemes for Hamilton-Jacobi equations on triangular meshes. *J. Comput. Appl. Math.* **167**, 227–241 (2004)
22. Lin, C.T., Tadmor, E.: High-resolution nonoscillatory central schemes for Hamilton-Jacobi equations. *SIAM J. Sci. Comput.* **21**, 2163–2186 (2000)
23. Lin, C.T., Tadmor, E.: L^1 -stability and error estimates for approximate Hamilton-Jacobi solutions. *Numer. Math.* **87**, 701–735 (2001)
24. Liu, Y.: Central schemes on overlapping cells. *J. Comput. Phys.* **209**, 82–104 (2005)
25. Luo, H., Xia, Y., Li, S., Nourgaliev, R., Cai, C.: A Hermite WENO Reconstruction-based discontinuous Galerkin method for the Euler equations on tetrahedral grids. *J. Comput. Phys.* **231**, 5489–5503 (2012)
26. Osher, S., Sethian, J.A.: Fronts propagating with curvature dependent speed: Algorithms based on Hamilton-Jacobi formulations. *J. Comput. Phys.* **79**, 12–49 (1988)
27. Osher, S., Shu, C.-W.: High-order essentially nonoscillatory schemes for Hamilton-Jacobi equations. *SIAM J. Numer. Anal.* **28**, 907–922 (1991)
28. Qiu, J.: WENO Schemes with Lax-Wendroff type time discretizations for Hamilton-Jacobi equations. *J. Comput. Appl. Math.* **200**, 591–605 (2007)
29. Qiu, J.: Hermite WENO schemes with Lax-Wendroff type time discretizations for Hamilton-Jacobi equations. *J. Comput. Math.* **25**, 131–144 (2007)
30. Qiu, J., Shu, C.-W.: Hermite WENO schemes for Hamilton-Jacobi equations. *J. Comput. Phys.* **204**, 82–99 (2005)
31. Shu, C.-W.: High order numerical methods for time dependent Hamilton-Jacobi equations, Technical Report 11. Institute for Mathematical Sciences National University of Singapore, Mathematics and Computation in Imaging Science and Information Processing (2007)

32. Tao, Z., Li, F., Qiu, J.: High-order central Hermite WENO schemes on staggered meshes for hyperbolic conservation laws. *J. Comput. Phys.* **281**, 148–176 (2015)
33. Tao, Z., Li, F., Qiu, J.: High-order central Hermite WENO schemes: Dimension-by-dimension moment-based reconstructions. *J. Comput. Phys.* **318**, 222–251 (2016)
34. Yan, J., Osher, S.: A local discontinuous Galerkin method for directly solving Hamilton-Jacobi equations. *J. Comput. Phys.* **230**, 232–244 (2011)
35. Zennaro, M.: Natural continuous extensions of Runge-Kutta methods. *Math. Comput.* **46**, 119–133 (1986)
36. Zhang, Y.T., Shu, C.-W.: High order WENO schemes for Hamilton-Jacobi equations on triangular meshes. *SIAM J. Sci. Comput.* **24**, 1005–1030 (2003)
37. Zheng, F., Qiu, J.: Directly solving the Hamilton-Jacobi equations by Hermite WENO schemes. *J. Comput. Phys.* **307**, 423–445 (2016)